AGU PUBLICATIONS

Water Resources Research

RESEARCH ARTICLE

10.1002/2013WR015117

Key Points:

- Experiments on how feed texture affects bed adjustments are conducted
- Bed surface evolution is highly dependent on the feed texture
- Gravel fraction in the feed influences how bed load approaches the feed texture

Supporting Information:

- Readme
- Detail of numerical code and figure and table captions
- Figure S1
- Figure S2
- Figure S3
- Table S1

Correspondence to:
C. Ferrer-Boix,
cfboix@geog.ubc.ca

Citation:
Ferrer-Boix, C., and M. A. Hassan (2014), Influence of the sediment supply texture on morphological adjustments in gravel-bed rivers, *Water Resour. Res.*, *50*, doi:10.1002/2013WR015117.

Received 27 NOV 2013
Accepted 14 OCT 2014
Accepted article online 16 OCT 2014

Influence of the sediment supply texture on morphological adjustments in gravel-bed rivers

Carles Ferrer-Boix[1] and Marwan A. Hassan[1]

[1]Department of Geography, University of British Columbia, Vancouver, British Columbia, Canada

Abstract The role played by the texture of the sediment supply on channel bed adjustments in gravel-bed rivers is poorly understood. To address this issue, an experimental campaign has been designed. Flume experiments lasting 96 h in a 9 m long, 0.60 m wide have been performed with different sand-gravel mixtures as feed textures. The response of the surface texture has been found to be highly dependent on the grain size distribution of the feed. When the feed texture included gravel, the finest fractions of the sediment supply infiltrate beneath the surface. Conversely, sand remains on the surface when the feed texture lacks gravel. This different textural response becomes obscured when water discharge increases. Further, the sediment transport rate approaches the feed rate differently depending on the content of gravel in the feed texture. When a small proportion of gravel is part of the feed texture, bed load transport rate asymptotically approaches the feed rate. However, when a significant fraction of gravel is part of the feed grain size distribution, bed load transport rate approaches the feed rate by following an oscillatory path. These findings have been verified in terms of a one-dimensional numerical model. This modeling reveals that the higher the differences in mobility among the grain sizes contained in the feed texture, the more evident is the nonasymptotic transient trend toward equilibrium.

1. Introduction

Bed load transport and surface texture in gravel-bed rivers interact in a manner which obscures determination of the cause and effect relationships [*Wilcock*, 2001]: do changes in bed load transport cause adjustments in surface texture or, conversely, do bed load changes arise from surface texture modifications? How the bed surface adjusts to different sediment supplies and textures is still an open question. In a feed experiment, the surface composition and the bed slope adjust through time so that the bed load transport rate and its texture match the feeding values at equilibrium [*Parker and Wilcock*, 1993; *Wilcock and DeTemple*, 2005]. However, it is still unknown how this evolution proceeds. This investigation focusses on studying the transient adjustments of the bed surface, bed load transport rates, and their grain size distribution to different sediment feed textures in gravel-bed rivers.

Gravel-bed rivers commonly have stable beds, with relatively little sediment mobilization even during high flows [*Church et al.*, 1998; *Church and Hassan*, 2002; *Hassan et al.*, 2008]. Under conditions of low sediment supply, it has been shown that gravel-bed streams commonly have a coarse armor which develops (i) as a result of horizontal sorting of fine material from the bed surface during small/intermediate flows that are incapable of mobilizing the coarser fractions [e.g., *Gessler*, 1970; *Parker and Sutherland*, 1990], or (ii) through vertical sorting during the movement of the coarse grains [e.g., *Parker and Klingeman*, 1982; *Rosato et al.*, 1987]. In turn, it has been hypothesized that bed structures (e.g., clusters and imbrication) develop under below-competent flows [*Haynes and Pender*, 2007; *Piedra et al.*, 2012].

Besides an impact on bed armoring, sediment supply plays a major role in bed stability and significantly impacts channel morphology. Frequency of sediment input events may temporally dominate channel processes and morphology, significantly changing sediment transport dynamics [*Hassan et al.*, 2008; *Madej et al.*, 2009; *Pryor et al.*, 2011]. Patterns of the quasi-cyclic channel response by which channel first aggrades to later degrade, associated with rapid inputs of sediment from external sources, have been described in a number of field observations and some experimental studies [e.g., *Hoffman and Gabet*, 2007; *Hassan et al.*, 2008; *Sklar et al.*, 2009; *Pryor et al.*, 2011; *Podolak and Wilcock*, 2013]. Changes in the magnitude of the sediment supply induce morphological responses in gravel-bed rivers. Particularly, a reduction of the sediment supply leads to a narrow zone of active transport within the channel which can degrade [*Dietrich et al*., 1989, 2005; *Nelson et al*., 2009; *Venditti et al*., 2012] if the sediment availability is well below the sediment capacity. Sediment supply also plays a central role in the spatial arrangement of bed surface patches [*Dietrich et al*., 1989, 2005; *Nelson et al*., 2009; *Venditti et al*., 2012].

Channel morphology and sediment mobility are also influenced by the texture of the supplied sediment. Coarser sediment supply than what the flow is competent to move will likely result in the development of an upstream sediment wedge, changing bed surface slope, and reducing sediment mobility [*Wilcock*, 2001]. Of particular, interest for this study is the proportions of sand and gravel fractions present in the supply compared to those fractions present in the surface, especially with regards the coarse material. Sand-sized sediment delivered to channels fills pore spaces and reduces pivot angles for gravel-sized grains being transported over the bed surface, which then are more easily mobilized [*Buffington et al*., 1992; *Wilcock*, 1998; *Curran and Wilcock*, 2005]. Additionally, *Venditti et al*. [2010] observed that smoothing of the bed surface by interstitial filling of fine material enhanced the mobility of the coarse particles by increasing the drag force exerted on them by the flow.

Researchers has also been conducted to study the effect of particle interactions on bed adjustments and temporal variations in bed load transport rates. Whereas *Whiting et al*. [1988] suggest that the formation of bed load sheets (thin, downstream migrating mass of sediment, the front edge of which is formed by coarse particles) could be due either to the patchy nature of fine-sediment infilling or to the concentration of coarse grains, *Nelson et al*. [2009] found that the ratio of coarse to fine gravel could play an important role in the formation of bed load sheets, the dynamics of which are determined by the sediment supply. *Iseya and Ikeda* [1987] found that bed load fluctuations or pulses could be partly due to a changing availability of bed material (longitudinal sorting). *Kuhnle and Southard* [1988] reported bed load fluctuations related to bed load sheets and dunes passing. It is worth mentioning that the bed load fluctuations reported in the experiments by *Iseya and Ikeda* [1987], *Kuhnle and Southard* [1988], and *Nelson et al*. [2010] were observed under equilibrium conditions. These aforementioned bed load pulses, often referred to as periodic variations of bed load [*Hoey*, 1992], differ from sediment waves, which are longer variations of bed load associated with sediment storage [*Gilbert*, 1917]. Thus, coarse material temporarily stored as a sediment wedge [*Wilcock*, 2001] can be interpreted as a downstream traveling sediment wave. However, what remains uncertain is how the interactions of grains of different particle sizes affect bed surface texture and bed load adjustments during the transient stage to equilibrium. As mentioned above, it is well established what bed load transport (rate and texture) is at equilibrium in flume experiments in which water and sediment are both fed at a constant rate. However, the influence of the texture of the sediment supply on the adjustments of the texture of the surface and the bed load transport rates and their grain size distribution during the transient stages toward equilibrium deserves more research. In this sense, it has been recognized that river response to disturbances may not be monotonic [*Hoey*, 1992].

This research has direct bearing on gravel-bed streams in which large amounts of external sources of coarse material can enter the river [*Benda and Dunne*, 1997]. In these cases, not only the final equilibrium state is important but also the transient stages are relevant. Since a considerable time interval may be needed to achieve equilibrium [*Hoey*, 1992], frequent episodic inputs of sediment may preclude attainment of equilibrium. To study these issues, flume experiments and a numerical model have been designed. The numerical model was conceived to complement the flume experiments. Therefore, it provides supporting evidence and helps to explain some of the results obtained from the flume experiments.

2. Experiments and Numerical Model Description

2.1. Experimental Design

A set of flume experiments, conducted in the Geography Department, Hebrew University, was designed to examine the influence of sediment supply texture on channel bed adjustment. Summary characteristics of the flow and sediment are provided in Table 1. The experiments were carried out in a 9 m long tilting flume, 0.60 m wide, and 0.50 m deep. The most upstream 1.0 m of the bed was fixed and immobile by using relatively large particles, equivalent to the D_{84} of the bed material. The experiments were carried out using a setup that had been well-verified in advance [*Hassan et al*., 2006]. A layer of 0.07 m deep loose material with specific gravity of 2.65 was placed along the last 8.0 m of the flume as the initial bed mixture (Figure 1).

Table 1. Experimental Hydraulic and Sediment Data[a]

Experiment	Q_w (m^3/s)	$q_{b,f}$ (g/m/s)	GSD Feed	$D_{50,f}$ (mm)	S_{b0}	τ_{b0} (Pa)	$D_{50,s}\|_{t=96\ h}$ (mm)	$q_{b,out}\|_{t=96\ h}$ (g/m/s)	$D_{50,b}\|_{t=96\ h}$ (mm)	$W_{b,T}$ (kg)
G1	0.021	0.00			0.0080	5.1	5.6	0.024	1.2	49
G2	0.032	0.00			0.0080	6.2	6.4	0.042	1.1	150
G3	0.021	0.14	Moved-1	1.5	0.0081	5.1	6.3	0.14	1.2	60
G4	0.021	0.36	Moved-1	1.5	0.0081	5.1	5.9	0.36	1.2	89
G5	0.021	0.49	Moved-1	1.5	0.0080	5.1	5.9	0.47	1.2	130
H1	0.032	0.35	Moved-2	1.5	0.0085	6.2	4.0	0.37	1.4	200
H2	0.032	0.55	Moved-2	1.5	0.0085	6.2	6.4	0.56	1.7	260
H3	0.032	0.75	Moved-2	1.5	0.0080	6.2	6.1	0.76	1.3	280
H4	0.021	0.16	Coarse	2.8	0.0085	5.1	7.1	0.059	1.1	57
H5	0.032	0.29	Coarse	2.8	0.0085	6.2	6.0	0.14	1.2	160
H6	0.032	0.54	Coarse	2.8	0.0085	6.2	6.5	0.36	1.3	210
H7	0.032	0.73	Sand	1.4	0.0085	6.2	1.9	0.89	1.2	300
H8	0.032	0.38	Sand	1.4	0.0085	6.2	5.0	0.55	1.4	240
H9	0.021	0.25	Sand	1.4	0.0080	5.1	2.4	0.26	1.4	96
I1	0.021	0.48	Sand	1.4	0.0080	5.1	2.0	0.55	1.2	140

[a] Q_w: water discharge, $q_{b,f}$: sediment feed rate (per unit with), GSD: grain size distribution, $D_{50,f}$: median grain size of the feeding texture, S_{b0}: initial bed slope, τ_{b0}: initial boundary shear stress; $D_{50,s}|_{t=96\ h}$ and $D_{50,b}|_{t=96\ h}$: median grain size of the bed surface and the bed load at the end of the runs (i.e., after 96 h). $q_{b,out}|_{t=96\ h}$ and $W_{b,T}$: unit bed load transport rate and total amount of sediment collected at the end the runs.

Before starting each run, the bed was slowly saturated and then drained to aid sediment settlement. Thirteen experiments were conducted in feed mode: water and sediment discharge were supplied under steady conditions from the flume inlet. Sediment feed rate per unit width $q_{b,f}$, ranged between 0.14 and 0.75 g/m/s. Two experiments were carried out under zero feed rate (Table 1). Runs were conducted using two water discharges which were chosen to be similar to water discharges at the beginning of the rising limb in a set of experiments with hydrographs [*Hassan et al.*, 2006]. Four different textures were used as the feed material (Figure 1): moved-1, moved-2, coarse, and sand. All these textures are unimodal: whereas peak frequencies for sand in moved-1 and moved-2 textures are associated with a grain size of $D = 1.41$ mm, peak frequency for the coarse texture is associated with a particle size of $D = 5.66$ mm. The sand content in the three finest textures ranges between 60% and 70% (it declines to 41% for the coarse grain size distribution). The median grain diameter of the coarsest texture nearly doubles those of the other three grain size distributions and whereas the geometric standard deviation of these three latter textures ranges between 2.1 and 2.4, it reaches a value of 3.4 for the coarsest grain size distribution. The median grain size, σ_g, 16% and 84% percentiles (i.e., 16% and 84%, respectively, finer than) as well as the sand content are listed in the figure inset. The sand and the coarse feeds represent the extreme grain size distributions (the latter being the same as the initial bed). Moved-1 and moved-2 textures were the grain size distributions of the bed load collected between 8 and 16 h in the two runs without feed under low and high flow conditions, respectively ($t = 16$ h was considered as the time for the surface texture adjustment [*Church et al.*, 1998] and $t = 8$ h was taken to have an intermediate measurement during the adjusting period). The duration of all runs was 96 h. The experimental procedures and the duration of the runs were the same as for the experiments of *Church et al.* [1998], *Hassan and Church* [2000], and *Hassan et al.* [2006]. The study follows previous research by *Church et al.* [1998] and *Hassan and Church* [2000]. They both modeled Harris Creek, British Columbia, Canada, under no feed conditions or feeding using moved textures. Harris Creek is a cobble-gravel-bed river and its hydrological regime is snowmelt-dominated; with a mean annual flow and maximum recorded flood of 19 and 35 m^3/s, respectively [*Church et al.*, 1998; *Hassan and Church*, 2000]. Channel width is of the order of 10 m, water surface slope ranges from 0.006 to 0.011, mean diameter of the subsurface material extends from 22 to 45 mm whereas mean surface material is ~64 mm in pools and 76 mm in riffles. Harris Creek is an upland stream with little sediment supply and well developed armored surface. Experiments in these previous studies were scaled using Froude similarity at 1:20; for more details see *Church et al.* [1998] and *Hassan and Church* [2000]. The bulk texture (i.e., the one used as the initial bed surface and as feed in coarse-supplied runs) was selected such that the grain size distribution extended from coarse sand to coarse gravel forming a poorly sorted mixture as of gravel-bed streams. For these given texture, flow conditions (water discharges, initial bed slopes) were selected in such a way partial transport (as defined by *Wilcock and McArdell* [1993]) occurred. Slightly higher feed rates than in previous research in Harris Creek [*Hassan and Church*, 2000] were chosen. Unimodal feed texture for sand-supplied runs was chosen as of that transported at low flow in Harris Creek [*Hassan*

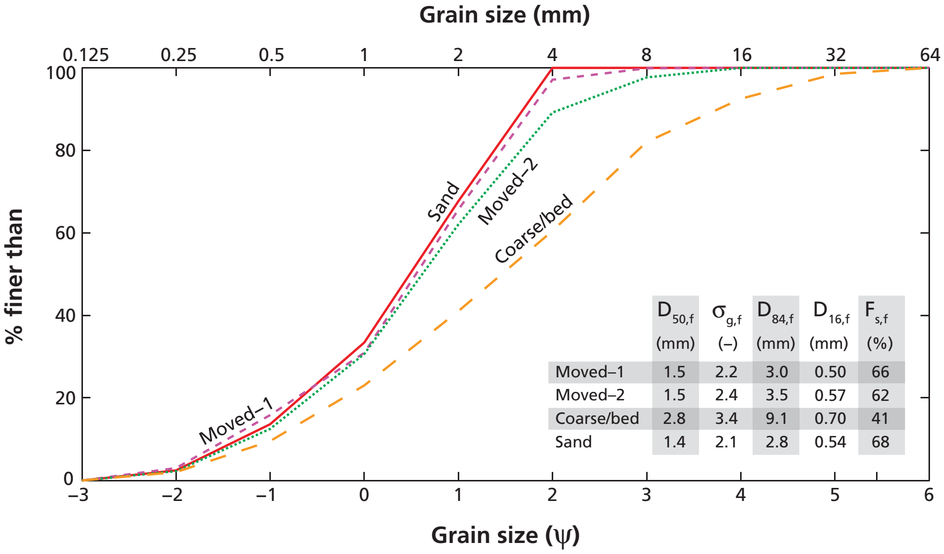

	$D_{50,f}$ (mm)	$\sigma_{g,f}$ (–)	$D_{84,f}$ (mm)	$D_{16,f}$ (mm)	$F_{s,f}$ (%)
Moved–1	1.5	2.2	3.0	0.50	66
Moved–2	1.5	2.4	3.5	0.57	62
Coarse/bed	2.8	3.4	9.1	0.70	41
Sand	1.4	2.1	2.8	0.54	68

Figure 1. Particle size distribution of feed textures used in the experiments. Note that the sediment mixture, i.e., the texture of the bed before commencing the runs is the coarse distribution. $D_{50,f}$: median grain size; $\sigma_{g,f}$: geometric standard deviation; $D_{16,f}$: 16 percentile of the feed texture; $D_{84,f}$: 84 percentile of the feed texture; and $F_{s,f}$: percentage of sand of the feed texture.

and Church, 2000]. Regardless of the experimental campaign was different in scope, it was conducted following as much as possible past research on East Creek so that results are still comparable. Although inspired by this past research, the experiments presented herein aimed to represent a general configuration of a gravel-bed stream rather than a specific field case.

Flow and sediment measurements were taken within a study reach between 4.75 and 5.25 m from the headbox. No water surface elevation was imposed at the outlet of the flume. Thus, a little acceleration of the flow was observed at the downstream end of the flume, which did not extend to the study reach. Sediment leaving the channel was collected in a trap at the end of the flume. At eight specified time intervals throughout the experiments, flow was lowered to a level below the initiation of motion of the particles for bed surface photography, bed surface sediment sampling, and sediment trap replacement. The volume of material collected at each specific time represents, thus, the mean bed load transport rate of the period of time during which the trap was filled. The bed surface was characterized based on two complementary methods: clay and color sampling [*Hassan et al*., 2006]. Clay samples were extracted using a piston device coated with clay [*Fripp and Diplas*, 1993] that was pressed onto the bed surface so that the bed material was embedded in the clay. The clay samples were taken downstream of the study reach. Bed load and clay samples were dried, weighted and sieved at 1/2 ψ intervals. The study reach was sampled by using an adaptation of the Wolman method based on color coded sediment at 1/2 ψ intervals, thus providing a noninvasive characterization of the bed surface in that area. Painting of each grain size was done manually by shaking a cylindrical receptacle containing the particles and the paint until it was visually observed that the paint uniformly covered the surface of the stones. Estimates of the initial boundary shear stress (Table 1) were obtained using the depth-slope method, taking the initial bed slope as the friction slope. It is assumed here that the depth-slope product is a reasonable proxy of the actual shear stress because the methodology yields an average value for the whole flume and the present investigation is focused on the overall adjustment of the channel in response to changes in the feed texture.

2.2. Numerical Model

A one-dimensional morphodynamic numerical model was developed to simulate the feed experiments. For this study, the normal flow approximation (steady and uniform) has been used to reproduce the water flow. A detailed description of the numerical model can be found in supporting information. As the experimental effort was of limited scope, a set of numerical experiments have been performed to confirm the influence of the feed texture in the evolution of the bed surface and bed load transport rates by considering more discharges, feed rates, and feed textures than provided by the experiments. The main goals of the numerical tests are: (i) to confirm the observations of the textural and bed load responses to the feed grain size distribution and (ii) to broaden the range of feed textures, water discharges, and feed rates to obtain a more general picture of how the bed surface and the bed load transport rate adjust to those parameters.

3. Results

The influence of the feed texture on bed adjustments is analyzed by selecting those representative experiments with the same water discharge and similar sediment feed rate, but with different feed textures (Table 1): runs G3 and H4, H2 and H6, and G5 and I1. The results of all other experiments are presented in Appendix A.

3.1. Experimental Observations

3.1.1. Sediment Transport

Figure 2 presents the temporal evolution of the ratio between sediment transport at the outlet of the flume and feed rates at the inlet for the six selected runs.

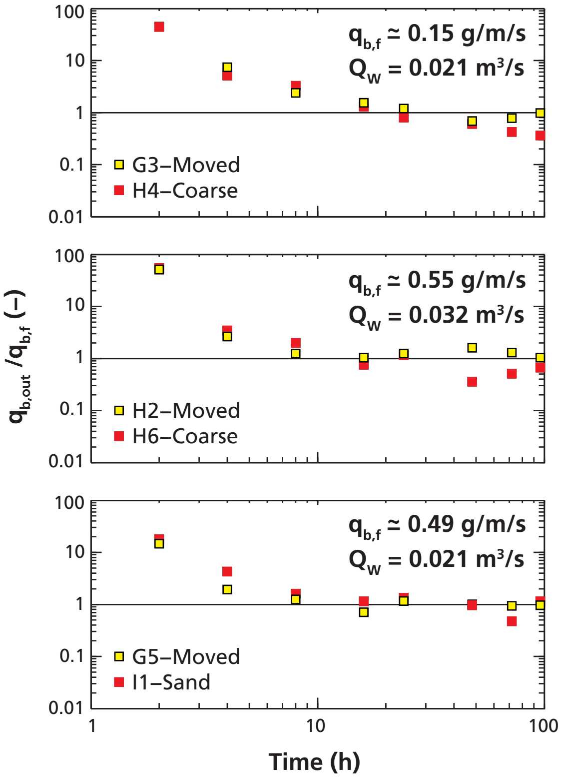

Figure 2. Evolution of the ratio between the bed load transport and the feed rates for runs G3 and H4, H2 and H6, and G5 and I1. The horizontal line: $q_{b,out}=q_{b,f}$.

Common trends during the first 20 h of the runs are observed in sediment transport rate for each pair of runs: the maximum difference between runs in each plot within this period of time is lower than 60%, except for runs I5 and G1 at $t=4$ h. This common path can be interpreted as an influence of the initial bed surface and bed slope on the bed load adjustments. High bed load transport rates during the first 16 h occur because of the initial high content of fine material on the bed surface which enhances the mobility not only of fine grain particles but also of the coarse fractions [*Curran and Wilcock*, 2005]. From this time onward, bed load transport rate is affected by both the water discharge and the feed rate and its texture.

As bed load inherently fluctuates, equilibrium is considered to be attained when consecutive measurements oscillate around the feed rate for an extended period of time. Except for the aforementioned bed load fluctuations, bed load transport rate in experiments fed with sand and moved material, regardless of the feed rate and the water discharge, asymptotically approaches the feed rate of each run, i.e., bed load transport gradually decreases until eventually reaching the feed rate within the 96 h of experiments. This is not the case in the coarse-fed runs in which an oscillatory (nonasymptotic) path is followed to reach the feed rate. This nonmonotonic trend toward the feed rate can be conventionally quantified by counting the number of points in the temporal evolution of the sediment transport rate in which the following conditions are satisfied: (i) bed load rate is below the feed (i.e., data points below 1 in Figure 2) and (ii) bed load still decreases. If these two simultaneous conditions are satisfied, bed load transport will have to rise in order to match the feed rate [*Parker and Wilcock*, 1993; *Wilcock and DeTemple*, 2005], and a nonasymptotic path will be followed to attain equilibrium. The average number of points that satisfy both conditions for coarse-fed runs equals 3 whereas a value close to 1 is obtained for the rest of the experiments, indicating a different bed load response toward equilibrium in coarse and fine (sand and moved) supplied runs. Sediment transport rate in fine-fed runs (i.e., supplied with sand and moved textures) starts to straddle equilibrium conditions after 16–24 h: the mean relative deviation of the bed load transport rate compared to the feed rate in these runs between $t=16$ h and $t=96$ h is 16%, which can be taken as a sign that these experiments had achieved

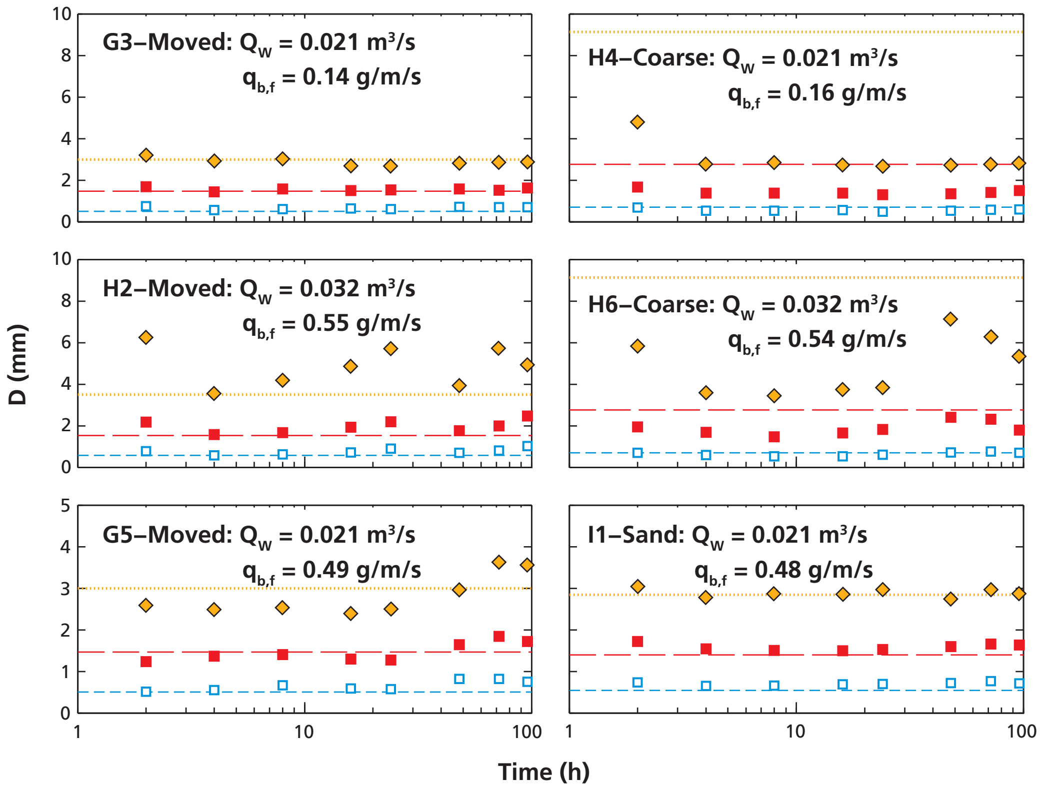

Figure 3. Bed load position statistics: $D_{16,b}$ (open squares), $D_{50,b}$ (filled squares), and $D_{84,b}$ (diamonds). Dashed lines illustrate the values of the percentiles for each feed texture.

equilibrium at $t = 96$ h. Bed load transport approaches the feed rate differently in coarse-supplied runs (H4 and H6). Bed load transport rate rapidly declined with time, reaching values lower than the feed rate (e.g., out/feed < 1) at $t = 16$ h. Bed load at the final stages of the experiments, mainly in run H4 but also in run H6, is below the feed rate (bed load at $t = 96$ h is 63% and 34% of the feed rate for each of these runs). Mean sediment transport rate for coarse-fed runs from $t = 16$ h to $t = 96$ h is 30% below the feed rate. The fact that the bed load transport at $t = 96$ h, along with the mean sediment transport rates after $t = 16$ h until the end of the runs are well below the feed rates mean that these runs were not at equilibrium at $t = 96$ h (although bed load transport rate for run H6 had almost matched the feed rate). Thus, if these runs had been longer, bed load would have had to rise in order to approach equilibrium. Comparing runs H5 and H6 (Figure A1), it is clear that with the higher feed rate (i) the earlier the sediment transport rate declines below the feed rate and (ii) the more rapidly it recovers toward equilibrium conditions.

Bed load percentiles ($D_{16,b}$, $D_{50,b}$, and $D_{84,b}$) for selected runs are presented in Figure 3. Despite the scatter, fine-supplied runs (moved and sand) illustrate that bed load statistics at the end of the runs are around those of the feed, confirming that these runs have achieved equilibrium: the median grain size of the bed load transport deviates 17% from that of the feed rate at $t = 16$ h to $t = 96$ h. The $D_{50,f}$ is rapidly attained regardless of the flow and the feed rates (some oscillations at high flow—run H2 and to a lesser extent in run G5—with respect to $D_{84,b}$ are noticed). Two-sample Kolmogorov-Smirnov goodness-of-fit tests have been carried out comparing each bed load sample with the feed texture in each run. These tests confirm that all bed load samples at $t = 96$ h of moved and sand-supplied runs (expect for that of run H2) are statistically the same at significance level of 0.05. However, since the null hypothesis (i.e., that the bed load sample is the same as the feed) is accepted in run H2 for all other bed load samples, particularly at $t = 48$ h and $t = 72$ h, achievement of equilibrium at the end of all fine-supplied runs is supported.

The evolution of the bed load texture in coarse-supplied runs is completely different with respect to the fine feed experiments. Again, the bed load texture does not approach that of the feed monotonically (by coarsening or fining). Instead, bed load texture first fines to (eventually) coarsen later on depending on the experiment conditions. The grain size distribution of the bed load is finer than that of the feed at any time for all runs. Starting from a grain size distribution finer than the feed texture ($D_{50,b}/D_{50,f}$ for runs H4 and H6 at $t = 2$ h are 0.62 and 0.72, respectively), bed load gets even finer (the average $D_{50,b}/D_{50,f}$ ratio for these two runs from $t = 4$ h to $t = 16$ h is 0.51 and 0.59, respectively) until occasionally it gradually starts coarsening (the same ratio for the entire period after $t = 16$ h is 0.51 and 0.74, respectively) depending on the run conditions (flow and feed rates). At $t = 96$ h, the ratio between the median bed load transport rate and the median of the feed rate ranges between 0.56 and 0.66 (the former corresponding to run H4, the latter to run H6). Bed load texture in run H6 reached its finest grain size distribution during the period from $t = 4$ h to $t = 24$ h, suggesting an influence of the initial conditions [*Haynes and Pender*, 2007]: all fractions of the initial loose bed surface were evacuated during the process by which the bed surface was being worked by the flow [*Hassan and Church*, 2000; *Church and Hassan*, 2002], and thus their mobility was gradually reduced. The coarse bed load fractions at $t = 2$ h and their subsequent fining until $t = 24$ h in coarse-supplied runs (Figures 3 and A3) respond to the evacuation of these fractions due to the increase of their mobility by the initial abundance of fine material on the surface [*Curran and Wilcock*, 2005]. Bed load texture in coarse-supplied runs coarsens from $t = 24$ h onward. The texture of the bed load in run H4 does not show any significant change after $t = 4$ h and bed load coarsening is clearly noticed after $t = 8$ h in run H6. The finer values of the bed load statistics of coarse-supplied runs compared to those of the feed in Figure 3 confirm that these runs were far from equilibrium at $t = 96$ h. Unlike fine-supplied runs, results of two-sample Kolmogorov-Smirnov goodness of fit tests for coarse-supplied runs at significance level of 0.05 confirm that bed load transport at the end of the runs is statistically different from that of the feed.

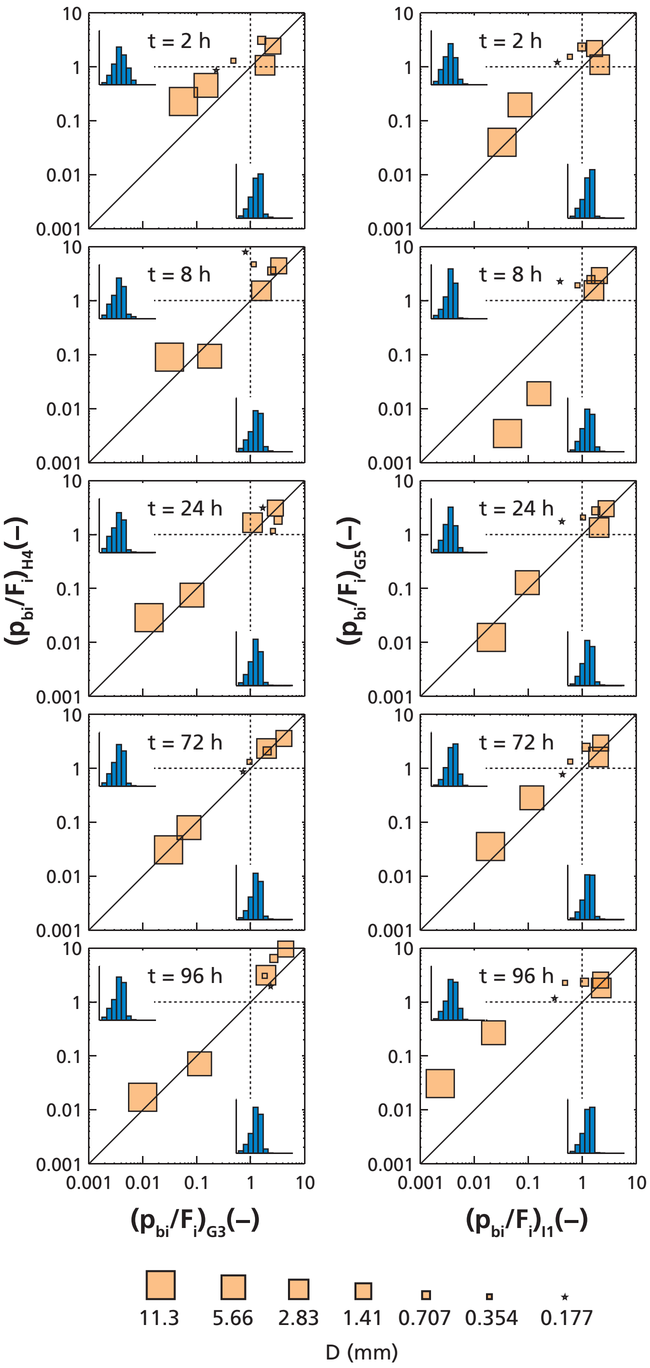

Figure 4. Comparison of fractional transport rates p_{bi}/F_i (p_{bi}, F_i: bed load and bed surface frequencies, respectively) evaluated at different times for runs H4 and G3 (left: $q_{b,f} \sim 0.14$ g/m/s, $Q_w = 0.021$ m^3/s and coarse and moved feed textures, respectively) and runs G5 and I1 (right: $q_{b,f} \sim 0.49$ g/m/s, $Q_w = 0.021$ m^3/s and moved and sand feed textures, respectively). Solid line indicates the equal line between vertical and horizontal axes. Dashed lines highlight full mobility ($p_{bi}/F_i = 1$). Histograms of bed load frequencies p_{bi} for each grain size have been added to each plot (top right corresponding to run H4—left column—and G5—right column—and bottom left to runs G3—left column—and I1—right column). The upper bound of the vertical axis is 0.45. Each bar in the histogram represents the frequency of the bed load for each grain size ($1-\psi$ apart) in increasing order.

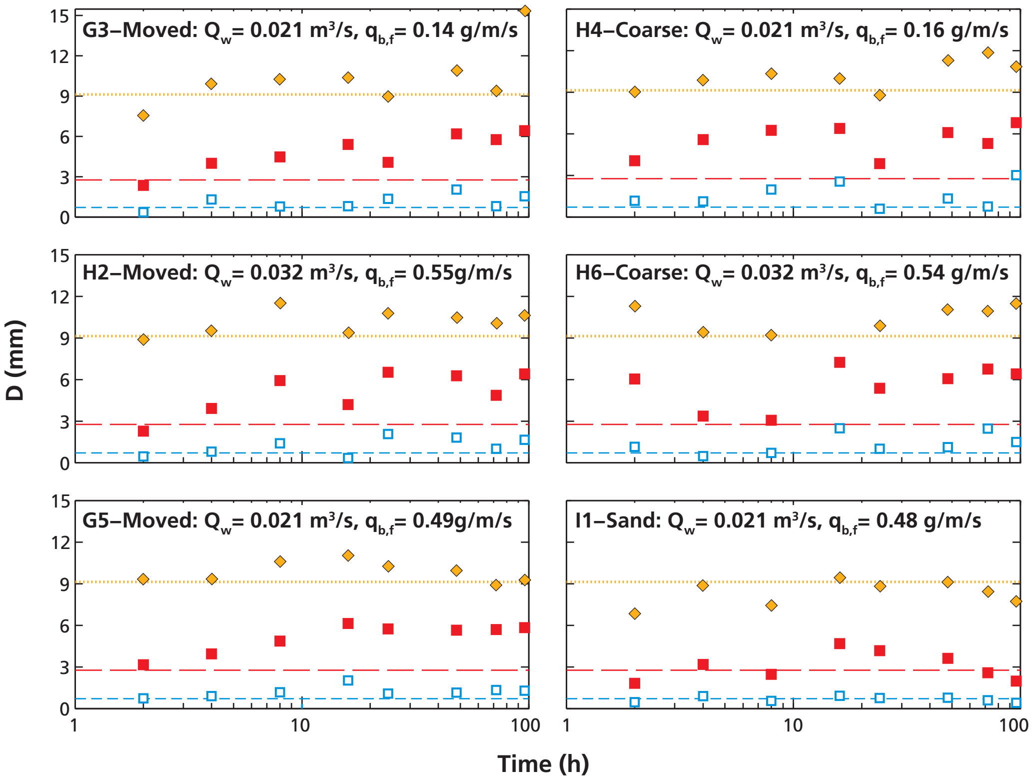

Figure 5. Surface position statistics: $D_{16,s}$ (open squares), $D_{50,s}$ (filled squares), and $D_{84,s}$ (diamonds). Dashed lines indicate the initial values of the respective percentiles. Each pair of plots in each row of the figure illustrates the results of two runs with the same water and sediment feed rate, but different feed texture.

Figure 4 presents the fractional transport rates by plotting the ratio of the bed load transport rate p_{bi} and surface fraction F_i for each grain size i. Since sediment available to be part of the bed load has its origin on the bed surface, p_{bi}/F_i indicates how over or misrepresented a certain grain size is in the bed load compared to its availability on the bed surface: sizes with lower mobility (usually the coarsest ones) gradually increase their presence on the surface until the bed load transport reaches the feed rate at equilibrium [*Wilcock and McArdell*, 1993]. Full mobility is achieved when $p_{bi}/F_i \geq 1$ [*Wilcock and McArdell*, 1993]. Each plot depicts the comparison of the fractional transport rates (at 1 ψ intervals) at a given time for a pair of selected runs with equal water discharge and sediment feed rate. The fractional transport rates at a given time range over 2 or 3 orders of magnitude. The maximum grain size initially present in the bed ($D = 45.3$ mm) was never present in the bed load measurements. The largest mobile particle increases with water discharge. Particles of $D = 22.6$ mm were only found in run G4 at $t = 2$ h when the bed surface was not worked by the flow. The fractional transport of the grain sizes most present in the bed load ($D = 1.41$ mm and $D = 2.83$ mm) does not apparently depend on the feed rate and its texture. Experimental results show that grain size of $D = 2.83$ mm is the boundary between full and partial transport [*Wilcock and McArdell*, 1993] (note that these data fall in the upper right quadrant of each plot).

All grain classes of the bed load finer than 5.66 mm are fully mobile at $t = 2$ h for run H4 (experimental results of the fractional transport of the two coarsest grain sizes for this run fall within an order of magnitude lower than $p_{bi}/F_i = 1$, therefore being partially mobile). Fractional transport rates of the two coarsest grain sizes collected in the sediment trap in fine-supplied runs(G3, G5, and I1) are partially mobile $-p_{bi}/F_i$ is between 1 and 2 orders of magnitude lower than 1$-$ at $t = 2$ h. From this time onward, particle mobility depends on the feed texture. Minor changes in relative mobility are observed in particles finer than 2.83 mm (fully mobile particles) in runs G5 and I1 at each time measurement (all data plot within a relatively narrow range above 1). However, the finest two grain classes in run I1 are systematically below 1. Mobility of partially mobile grain classes ($D \geq 5.66$ mm) in run G5 decreases from $t = 2$ h to $t = 8$ h, and gradually increases afterward until the end of the run. Mobility of these latter grain sizes in run I1 gradually and continuously declines from $t = 2$ h to $t = 96$ h.

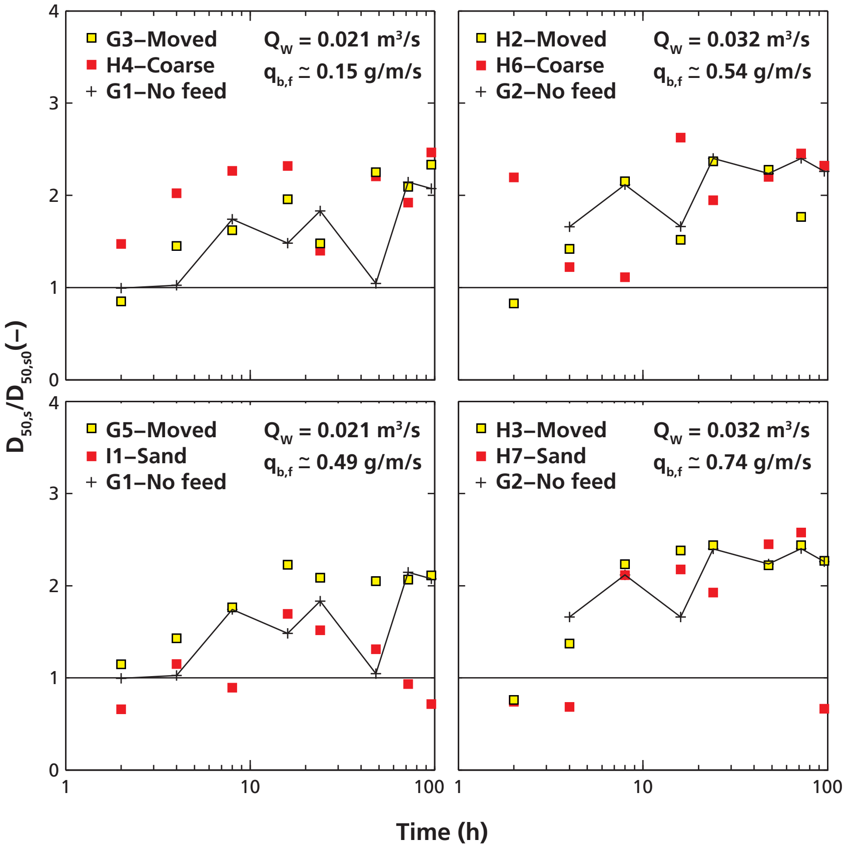

Figure 6. Ratio of the median surface diameter with respect to the initial one for selected runs. Surface coarsening data of no feed runs are included for comparison. The horizontal line defines no coarsening $D_{50,s} = D_{50,s0}$.

The relative mobility of coarse and moved experiments (G3 and H4) is similar (data approximately plot along the equal line of each plot). Except for the two finest grain sizes of run G3 (for which the fractional transport fall within an order of magnitude lower than $p_{bi}/F_i = 1$) grain sizes finer than $D = 2.83$ mm are fully mobile ($p_{bi}/F_i \geq 1$); the mobility of the two partially mobile grain sizes ($D \geq 5.66$ mm) reduces gradually as time passes.

3.1.2. Bed Surface Adjustments

Temporal evolution of the $D_{16,s}$, $D_{50,s}$, and $D_{84,s}$ of the bed surface for selected runs is presented in Figure 5. Bed surface adjustments apparently do not depend on the feed rate in moved-supplied runs under low flow (runs G3–G5). $D_{50,s}$ increasingly coarsens during the first 16 h of runs and reaches a constant value between 5.0 and 6.0 mm: the average $D_{50,s}$ from $t = 16$ h to $t = 96$ h in these two runs is 5.7 mm (the mean standard deviation is 0.56 mm). Less evident coarsening is observed with regard to $D_{84,s}$: this grain size gradually coarsens until $t = 16$ h; from this time onward, whereas $D_{84,s}$ for run G3 remains constant (despite the oscillations), it gets slightly finer for run G5 (this fining is clearly observed in the last two measurements). However, the mean value $D_{84,s}$ for the last five measurements is between 24% and 11% coarser than the D_{84} of bulk material in runs G3 and G5, respectively. Mean coarsening of the finest percentile D_{16} is between 78% and 87% in both runs for the period after $t = 16$ h. The armor ratio at the end of the runs G3 and G5 ranges between 2.1 and 2.4 (Figure 6). The same trend is observed in high flow moved-supply runs in Figures 5, 6, and A3.

The bed surface in coarse-supplied runs in Figure 5 (and also in Figure A3) generally coarsens with time until $t = 16$ h: starting from a median surface grain size at $t = 2$ h ranging between 2.2 mm (run H5) and 6.0 mm (run H6), it gradually increases up to a range between 6.4 mm (run H4) and 7.3 mm (run H5) at $t = 16$ h ($D_{50,s} = 7.2$ mm for run H6). From this time onward, the median surface grain size is maintained constant or even gets finer: the average $D_{50,s}$ from $t = 16$ h to $t = 96$ h in runs H4 and H6 are 5.7 mm and 6.4 mm, respectively (the standard deviation is 1.2 and 0.72 mm, respectively).

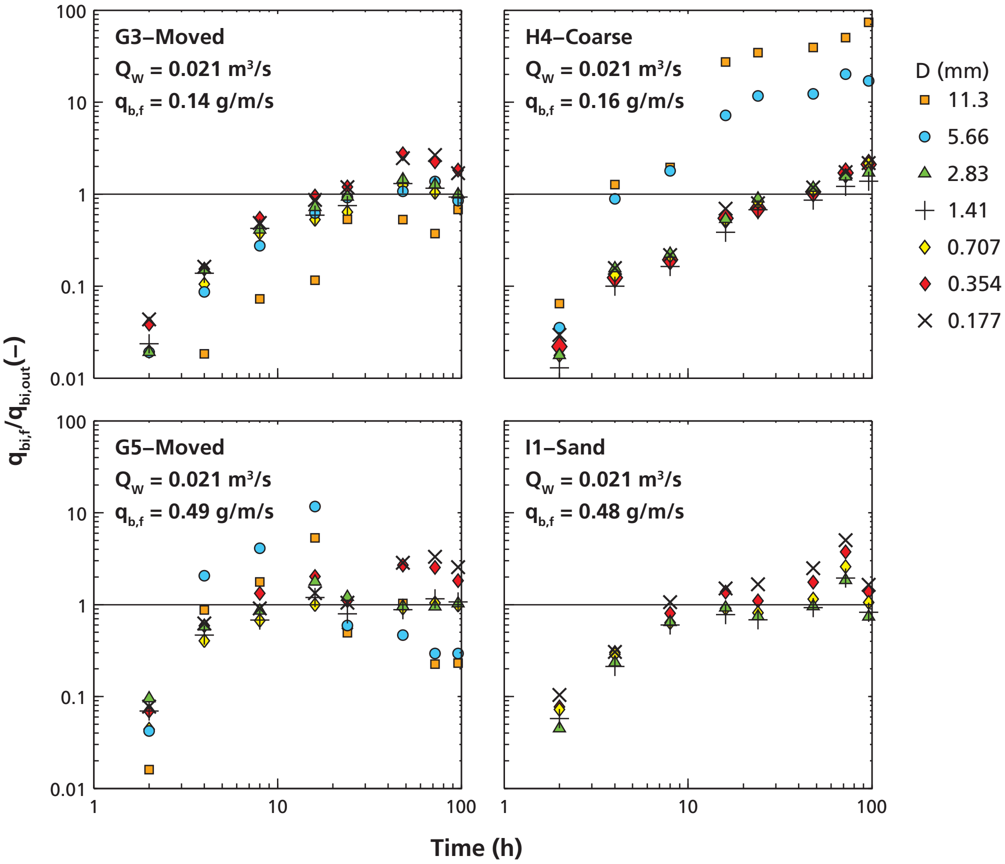

Figure 7. Storage/release ratio for each grain size for the selected runs. The horizontal line defines *i*-th bed load transport equal to the *i*-th feed rate ($q_{bi,out} = q_{bi,f}$).

An influence of the feed texture on the surface grain size distribution is noticed by comparing runs G5 and I1. Despite the minor differences in their feed texture (Figure 1), a different evolution is observed in both experiments. In both runs, the bed surface gradually coarsens until $t = 16$ h. From this time onward, the bed surface in run G5 remains approximately stable while it gradually fines in run I1 until becoming even finer than the bulk material. Figure 6 illustrates the changes in armoring for the selected runs.

Finally, the bed surface in sand-fed runs may depend on the water discharge. Although it is acknowledged that no sand runs with equal feed rate and different flow discharge were conducted, the dependence of the surface evolution on the water discharge can be observed in Figure 6 by comparing the evolution of the armor ratio in runs I1 and H7 but also in Figure A3 (comparing runs H7 and H8—high flow—and run I1—low flow and feed rate between those of runs H7 and H8). Experiments conducted at low flow show little coarsening (average $D_{50,s}$ after $t = 16$ h is 3.7 mm, with the mean standard deviation equal to 1.26 mm). However, the bed surface coarsens as much as the rest of the experiments in sand-supplied runs at high flow for the same period of time (median surface diameter for these runs ranges between 5.7 and 6.2 mm, with the average standard deviation of 1.6 mm).

3.1.3. Sediment Budget

A grain size specific sediment budget is evaluated by the ratio of the sediment transport rate at the flume outlet and the feed rate (*i*-th storage ratio). Two pairs of representative runs have been selected.

The mixture textures ranged between 0.177 and 45.3 mm, and 22.7 mm particles were rarely reported in the bed load texture (45.3 mm particles were not registered in any samples). This occurred regardless of the feed texture, even though those grain sizes represented 7.5% of the coarse texture (Figure 1). Consequently when forming part of the feed texture (coarse and moved-supplied runs), this material was stored in the flume. Most of this coarse material was stored as a wedge in the upstream part of the flume which was being transported—translated or dispersed [*Cui et al.*, 2003a, 2003b; *Sklar et al.*, 2009]—along the flume as time passed. Obviously, there was no storage of coarse material in sand-supplied runs, since it was absent from the feed texture.

Figure 7 shows the temporal evolution of the *i*-th storage ratio. This ratio for the two coarsest grain sizes of the feed ($D = 11.3$ and 5.66 mm) for run G3 is mostly below one (except at $t = 48$ h and $t = 72$ h when the storage ratio is slightly above 1 for $D = 5.66$ mm), i.e., more particles of this caliber leave the flume than enter. Conversely, the bed load transport rate of these grain sizes only exceeds the feed rate during the first 4 h in run H4, i.e., these particles are being stored in the flume afterward. Grain sizes finer than $D = 5.66$ mm in run H4 were evacuated from the flume during the first 24 h of the run and stored afterward. The storage in the flume of the coarsest fractions in runs H4 and H6 (coarse-supplied experiments) is also observed in Figure 3—compare the D_{84} of the bed load to that of the feed.

The influence in the bed surface and in the bed load transport rate of a small proportion of gravel in the feed texture is analyzed by comparing runs G5 and I1. Figure 7 shows that central grain-size classes in run G5 ($D = 0.707$–2.83 mm) approach the feed rate asymptotically. Coarser fractions, however, are stored from $t = 4$ h to $t = 16$ h contributing to the surface coarsening (Figure 2). From $t = 24$ h onward, more coarse particles leave the flume than enter. This process occurs contemporaneously with bed surface storage of the finest grain-size classes. All grain sizes of the bed load approach those of the feed texture in run I1 (bottom right). However, fine grain sizes are stored in the flume after $t = 48$ h in this run.

3.2. Numerical Results

The comparison of the results predicted by the numerical model and the experimental measurements can be found in supporting information (text and Figures S1, S2, and S3). In this section, only the numerical tests used to interpret the experimental campaign are presented. Channel adjustments to feed texture are analyzed by means of the evolution of the mean boundary shear stress and the bed elevation.

Figure 8 presents the numerical results of the evolution of the mean boundary shear stress and the bed elevation in the channel inlet predicted by the numerical model for two selected pairs of runs with equal water discharge and feed rate, but different texture: $Q_w = 0.021$ m^3/s, $q_{b,f} \cong 0.15$ g/m/s for runs G3 and H4 and $Q_w = 0.032$ m^3/s, $q_{b,f} \cong 0.54$ g/m/s for runs H2 and H6. Figure 8 (top) compares the temporal evolution of the Shields shear stress associated with the geometric mean diameter τ_g^* over the reference shear stress for the D_{84} τ_{rs84}^*. The Shield number associated with the geometric mean diameter is defined as

$$\tau_g^* = \frac{\tau_b}{\rho R g D_{g,s}}$$

where τ_b is the boundary shear stress, ρ is the water density, R is the submerged specific gravity, g is the acceleration of gravity, and $D_{g,s}$ is the geometric mean diameter of the surface. τ_{rs84}^* has been obtained using the expression of the hiding function proposed by *Wilcock and Crowe* [2003]. The latter reference dimensionless shear stress has been included since this analysis aims to study the role played by the coarsest fractions on the bed surface on the bed adjustments. An increase in the reference shear stress for the D_{84} occurs when the bed surface coarsens increasing thus the strength of the river bed to degrade: under equal flow conditions, the coarser the surface the lower the ratio (this conclusion can be nuanced under conditions of equal mobility, i.e., when the reference shear stress is maintained constant regardless of the grain size). Thus, under equal flow conditions, the lower the shear ratio the lower the sediment mobility of the coarse fraction of the mixture (here associated with D_{84}). The bottom plots present the numerical results of the temporal evolution of the bed elevation at the same station. Left and right plots compare the results of low and high feed rates, respectively. Figure 8 shows a decline of the shear ratio of approximately 76% during the first 16 h for all runs, regardless of the water discharge, and feed (rate and texture). This means that no different trends of the surface coarsening (that would be embedded in τ_{rs84}^*) occurred during the first 16 h of runs. Again, this suggests an effect of the initial surface condition: the influence of the fine loose material on the bed surface available to be transported dominates the channel response by exhibiting a common trend in the mobility of coarse fractions for runs G3 and H4 and H2 and H6, respectively. Different trends are observed in the shear ratio after $t = 16$ h depending on the feed texture: in moved-supplied

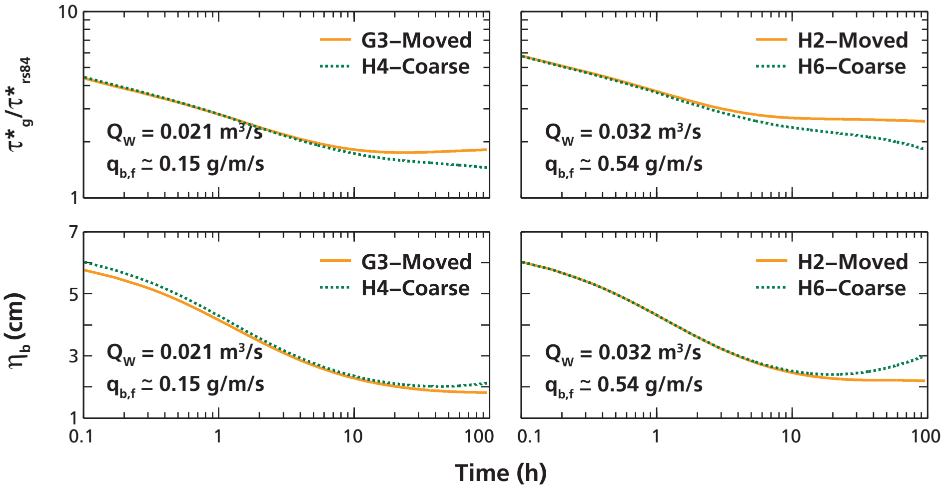

Figure 8. Temporal evolution of the ratio of the Shields stress associated with the geometric mean diameter over the dimensionless reference shear stress associated with D_{84} (top) in the flume inlet. (bottom) Temporal evolution of the bed elevation in the channel inlet. Comparisons are done for two pair of runs with equal water discharge, similar sediment feed, but different feed texture: (left) $Q_w = 0.021$ m^3/s, $q_{b,f} \cong 0.15$ g/m/s for runs G3 and H4 and (right) $Q_w = 0.032$ m^3/s, $q_{b,f} \cong 0.54$ g/m/s for runs H2 and H6.

runs, the drop in the shear ratio from $t = 16$ h onward is of 8% (this percentage rises to 20% for coarse-supplied runs in which a gradual decline is noticed after $t = 16$ h).

Numerical simulations show that, regardless of the feed texture, bed elevation during the first 16 h of runs degrades up to 67% of the initial bed elevation. Bed elevation of the channel inlet in moved-supplied runs remains mostly unchanged once the shear ratio stabilizes after $t = 16$ h: bed elevation at the end of the runs degraded 9% with respect the bed elevation at $t = 16$ h. No significant differences in the bed elevation between coarse and moved-supplied runs at low flow (G3 and H4) are observed. Minor differences in bed elevation are noticed between each set of compared runs until $t = 30$ h, again reflecting an influence of the initial conditions: the initial high rates of sediment leaving the flume due to the initial high content of sand on the surface were not balanced by the feed rate (Figures 2 and A1), and thus lead to rapid degradation of the bed, regardless of the texture of the feed. The inexistent influence of the feed texture on the evolution of the long profile during the first hours of the runs (also noticeable on the adjustments of the feed rate, its texture and on the evolution of the bed surface) reflect the role played the initial abundance of fine material on the surface, reducing bed irregularities and enhancing the mobility of coarse particles [*Venditti et al.*, 2010]. The lack of influence of the feed texture on the channel adjustments during the first hours of the runs is due to the relatively low sediment transport rates used in the experiments, typical of gravel-bed streams [*Church et al.*, 1998; *Church and Hassan*, 2002; *Hassan et al.*, 2008]. From $t = 30$ h time onward, bed elevation starts to aggrade in run H6, compared to run H2, the elevation of which remains unchanged. The new stage of channel aggradation is related to the reduction in the shear ratio after $t = 16$ h. This decline in the shear ratio leads to a decrease in the bed load transport of the coarsest fractions that deposit in the uppermost part of flume (Figure 7). This aggradation is in fact the sediment wedge that was observed during the experiments. Note that the aggradation predicted by the numerical model occurs simultaneously with the drop of the bed load transport below the feed rate in Figure 2.

Figure 9 presents the numerical results of the bed load transport rate over the feed rate ratio for the five textures considered in the inset plot, keeping water discharge ($Q_w = 0.032$ m^3/s) and feed rate ($q_{b,f} = 0.55$ g/m/s) constant. A surrogate for the dimensionless flow intensity q_w^* is defined by the Einstein number:

$$q_w^* = \frac{Q_w}{\sqrt{gRD_{g,f}D_{g,f}^2}} \qquad (1)$$

where g is the acceleration of gravity, R is the submerged specific gravity of sediment, and $D_{g,f}$ is the geometric mean diameter of the feed. Numerical results confirm the observations regarding the evolution of the bed load transport rate toward equilibrium: the lower the dimensionless flow strength (the coarser the

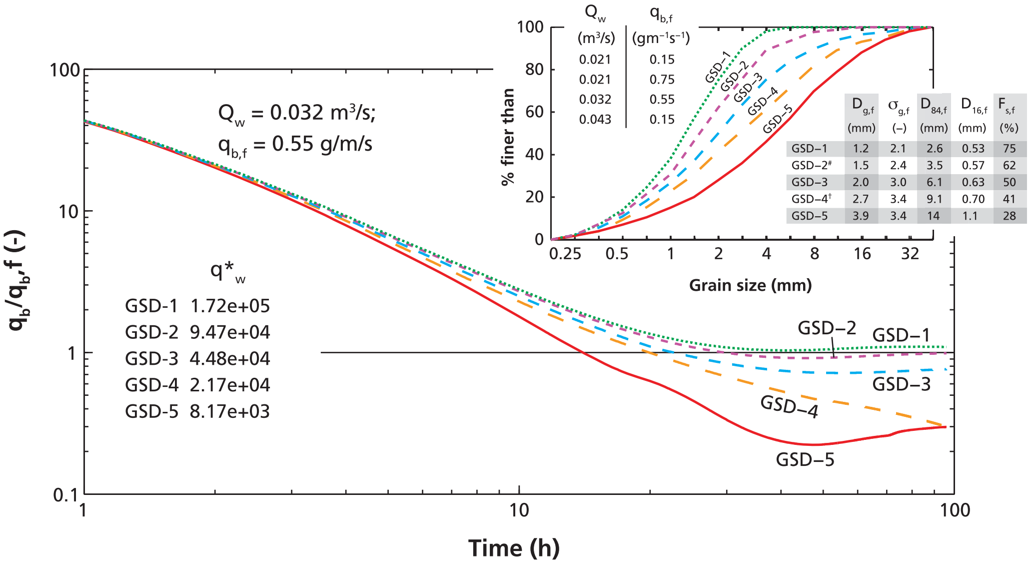

Figure 9. Predicted ratio of the bed load transport rate at the outlet of the flume and the feed rate for the five feed textures used for the following pair of water discharge and feed rate: $Q_w = 0.032$ m³/s, $q_{b,f} = 0.55$ g/m/s (indicated in bold text in the small table in the top right plot). The horizontal line defines bed load transport equal to the feed rate. Values of q^*_w for the given pair of Q_w and $q_{b,f}$ are inserted. The horizontal line indicates where $q_{b,out} = q_{b,f}$. Top right plot illustrates the percent finer of the five grain size distributions used in the numerical experiments with the most important statistics and the pair of water and sediment discharges used for each texture. (#: moved 2; †: coarse/bed, Figure 1).

feed rate), the larger the decline of the sediment transport rate below the feed rate. Thus, for the given flow conditions, the coarser the feed texture the less asymptotic the response of the bed load adjustments. This was observed in Figure 2 (runs G3–H4 and H2–H6).

4. Discussion

4.1. Temporal Adjustments

Differences in surface texture in runs G5 and I1 (evident from Figures 5 and 6) highlight the influence of a small proportion of gravel in the feed grain size distribution on channel adjustments. Figure 7 shows that coarser fractions were stored in the flume until $t = 16$ h contributing to the surface coarsening in run G5 (Figure 5). From $t = 24$ h onward, whereas more coarse particles left the flume than entered, the finest grain classes were stored in the flume. As the texture of the surface roughly remained stable after $t = 24$ h in run G5 (Figure 5), it can be indirectly deduced that the fine grain sizes infiltrated underneath the surface. Figure 4 (right) illustrates that fractional transport of the finest grain classes in run G5 remained stable over time (similar magnitude, and grouped within a relatively narrow and roughly horizontal band in each plot). This confirms that the fine material stored in run G5 was infiltrating underneath the surface. If these grain sizes had been stored on the surface, a reduction in the relative mobility would have been noticed in Figure 4 (by means of a downward sloping trend toward the finest fully mobile grain classes). Likewise, the finest grain sizes in run I1 were stored in the bed after $t = 48$ h (Figure 7), while bed load texture remained stable (Figure 3, right) and a moderate increase of the finest grain sizes in the bed surface was noticed (Figures 5 and 6). This suggests that the finest grain classes remained hidden behind the coarsest fractions on the bed surface. The simultaneous drop in the relative mobility of the two finest grain classes after $t = 24$ h (Figure 4) and the lack of variation of $D_{16,b}$ during the same period of time strengthen the analysis that fine material remained on the bed surface. The same indirect reasoning was followed by *Pender et al.* [2001] to determine whether fine material had infiltrated or remained hidden on the surface. The surface fining in run I1 after $t = 16$ h is also illustrated by the decrease in the armor ratio in Figure 6. Figures 5 and 7 illustrate that, after $t = 48$ h, along with a relatively stable surface texture (coarser than the bulk material), the finest grain classes in runs G3 and H4 were being stored in the flume. That would imply that these particles were infiltrating as in run G5. Infiltration of fine material and bed aggradation is synchronous in coarse-supplied runs (Figure 8), as observed by *Wooster et al.* [2008].

The most likely explanation of this divergent channel response is that the larger number of coarse particles on the bed surface in moved and coarse-supplied runs increases the probability of kinematic sorting of the fine grain sizes that controls the armor development [*Rosato et al*., 1987; *Wilcock et al*., 2001]. *Whiting et al*. [1988] hypothesized that interactions between sand and gravel grains could lead to the infiltration of sand between gravel interstices [*Iseya and Ikeda*, 1987] and hence make the gravel experience increasing drag force. In particular, the small increase in the proportion of coarse material in the feed texture in run G5 compared to the feed texture in run I1 (grain sizes in the feed coarser than 4 mm, absent in run I1, represent 3% of the feed in run G5) prompts coarser sediment on the bed surface, stimulating the infiltration of fine material underneath the coarse framework. This response is also observed in coarse-supplied runs. In this sense, it can be speculated that the surface coarsening in run I1 during the first 16 h of the run and the subsequent surface fining (Figure 6) were caused by the infiltration of fine supplied material underneath the coarse surface framework during the surface coarsening phase and remained hidden behind the coarse material in the surface after near-surface pores were clogged with fine material [*Frostick et al*., 1984] in the fining stage. Along with the fine infiltration, the sand-supplied texture in run I1 enhances the entrainment of the coarsest fractions on the surface that were not buried [*Wilcock*, 1998; *Curran and Wilcock*, 2005; *Venditti et al*., 2010] thus contributing to surface fining. This process explains the surface fining in run I1 after $t = 16$ h (Figure 6). Figure 6 also shows that the fine material stored in the surface is evacuated when the flow and the feed rate increases (run H7), driving coarsening of the bed, in accordance with the observations of *Lisle* [1989] in Northern California rivers where infiltration of fine sediment decreased with increasing bed load transport. Finally, Figure 6 (and also Figure 5) demonstrates that, despite local variations, no persistent trend in surface coarsening development is observed in moved and coarse-supplied runs after 16 h. Notably, *Church et al*. [1998] noticed no significant changes in the surface texture after 24 h, and in a set of runs to study the development of bed structures. In this regard, bed structures formed by particle sizes of $D = 5.66$ mm and $D = 11.3$ mm, were mostly observed in our experiments under no feed conditions and those supplied with coarse material; conversely, in moved and sand-supplied runs under low flow, some little structures were discerned; some of these structures were buried by the high content of sand on the surface in sand-supplied runs. *Hassan and Church* [2000] reported that major changes in the surface texture occurred within the first 16 h and little change from this time onward.

Bed load transport rate measurements in coarse-supplied runs do not asymptotically approach the feed rate (Figures 2 and A1). This response is hinted at in runs H4 and H5, in which bed load transport declined below the feed rate at $t = 24$ h and continued falling until the end of the runs. Bed load measurements dropped below the feed rate in run H6 from $t = 24$ h (or even 16 h) to $t = 48$ h and started to increase from this time onward, but without reaching the feed rate at the end of the experiment. Thus, equilibrium was not achieved in coarse-supplied experiments. Bed load measurements in these latter runs highlight an oscillating path toward equilibrium. *Parker et al*. [1982] reported the same evolution but their experiments ended at an equilibrium state. These oscillations were not related to the migration of small-amplitude bed forms or bed load sheets [*Iseya and Ikeda*, 1987; *Kuhnle and Southard*, 1988; *Whiting et al*., 1988], which were not observed during our runs. When the feed rate texture is better sorted (sand and moved-supplied runs) the evolution of the bed load toward equilibrium appears to be asymptotic, although some oscillations were observed, especially in the moved-supplied experiments at low flow (runs G3 and G5; Figure 2). Equilibrium was achieved in these runs at $t = 96$ h.

Differences in mobility among the supplied grain sizes for a given flow condition may be a possible reason for the oscillatory evolution of the bed load transport rate observed in coarse-supplied runs. For this discussion, let us consider an arbitrary texture of the feed mixture composed of only two sizes. If the initial bed surface is not worked, it is assumed that both the fine and the coarse fractions of the sediment transport will be relatively high during the first stages of the run compared to the feed rate because of the abundance of fine material on the bed surface and its influence on the enhancement of the coarse sediment transport rate [*Curran and Wilcock*, 2005]. Bed load transport rates higher than the feed rates during the early stages have been reported in our experiments (Figures 2, 7, and A1) and in previous similar research [*Hassan and Church*, 2000]. Thus, the bed profile and surface will gradually degrade and coarsen [*Parker et al*., 1982]. Channel degradation and bed surface coarsening will lead to a progressive reduction of the relative mobility of the coarsest fraction on the surface. As a result, a downstream propagating peak of the coarsest fraction of the bed load followed by a trough will be expected. The proportion of the coarsest fraction will rise again when the flow is capable of transporting the coarse material supplied (that has been stored in the uppermost reach of the flume increasing the bed slope, and thus the bed shear stress). The less mobile the coarse fraction the more time the perturbation would need to propagate along the flume. Figure 10 plots the

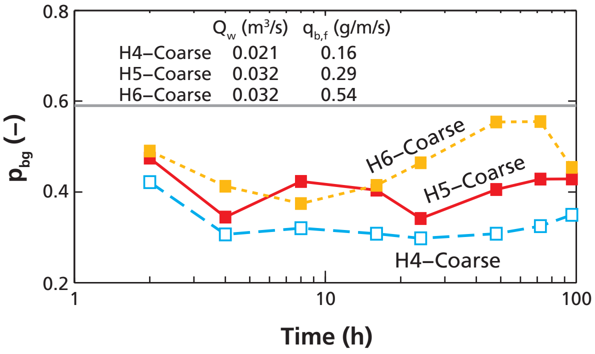

Figure 10. Temporal evolution of the fraction of gravel of the bed load measured during coarse-supplied runs. Horizontal line indicates the fraction of gravel of the feed rate in these runs (Figure 1).

gravel fraction of the bed load transport in all coarse-fed runs compared to the fraction of gravel supplied. Despite the scatter, data plotted in Figure 10 reproduce the aforementioned bed load adjustment process: the fraction of gravel in the bed load is initially high, it declines later on and rises again toward the end of the experiments. The peaks of the gravel fraction in Figure 10 represent the passage of waves of coarse material. Figure 10 demonstrates that for a given water flow and feed texture, the higher the feed rate the earlier the increase in the coarse fraction of the bed load transport rate. Conversely, the results of the coarse-supplied runs suggest that, for a given water flow, the magnitude of the gravel peaks decreases with the feed rate (compare the through of the curves of runs H5 and H6). No concluding results can be extracted with regards of the influence of the water discharge on the proportion of gravel in the bed load. However, higher flows lead to faster channel responses and thus, it can be hypothesized that higher water discharges drive to an earlier increase of the coarse fraction of the bed load toward the end of the runs. Following the same reasoning, it can be surmised that the higher the feed rate and the water discharge, the more frequent the pulses of coarse material.

The morphological result of this evolution is that different mobility rates of sand and gravel may cause bed load transport to eventually drop below the feed rate, in an oscillating process toward equilibrium. The larger the proportion of the coarsest fraction in the feed rate (compared to the finest fraction) the lower the sediment transport rate compared to the feed (this would explain why no decline below the feed rate is observed in moved-supplied runs). A decline of the bed load transport rate below the feed rate has been reported in our experiments (Figure 2). It is hypothesized that the higher the difference between relative mobility among grain classes in the texture of the sediment supply, the more time will be needed to reach equilibrium and the higher the amplitudes of the oscillation path. This hypothesis will be discussed based on the results of the numerical model.

4.2. Numerical Results

To start with a simple case, runs H5 and H6 have been simulated considering that all textures (feed, surface, and bulk material) are composed of a mixture of only two grain classes: $D_{\min} = 0.84$ mm and $D_{\max} = 4.8$ mm, such that the sand content is the same as in the experimental runs, $Fs = 41\%$ (Figure 1). Figure 11 illustrates the numerical results of the evolution of the ratio of the coarser fraction of bed load $p_{b,c}$ over that of the feed $p_{f,c}$ (top) and the ratio of the sediment transport and the feed rate (bottom). Figure 11 (top) qualitatively reproduce the experimental evolution of the sediment pulses (expressed in terms of the gravel fraction of the bed load transport rate): at a particular flume station, the proportion of gravel in the bed load initially increases; it declines later on until rising again toward the end of the runs. Further, the numerical results show that for a given water discharge and feed texture, the higher the feed rate: (i) the earlier the gravel pulses start, (ii) the lower the amplitude of these pulses, and (iii) the higher their frequency (equilibrium is attained earlier). However, while numerical results in Figure 11 support the evolution of the coarse fraction of the bed load described in the previous section (and the decline in the bed load transport below the feed rate), they do not provide a successful explanation of bed load oscillations registered in coarse-supplied runs in Figure 2 and numerically reproduced in Figures 9 and 10.

Since the ratios of the proportion of sand and gravel between the bed load (p_{bs} and p_{bg}) and the feed rate ($p_{bs,f}$ and $p_{bg,f}$) must tend to one at equilibrium, they can be used as an indicator of the achievement of this equilibrium.

Figure 12 illustrates the evolution of the ratio between the sand and gravel fraction of the bed load at the outlet over those of the feed texture, obtained by the numerical model under the following conditions: $Q_w = 0.032$ m^3/s, $q_{b,f} = 0.55$ g/m/s. Some features can be noticed: (i) the higher q_w^*, i.e., the finer the feed

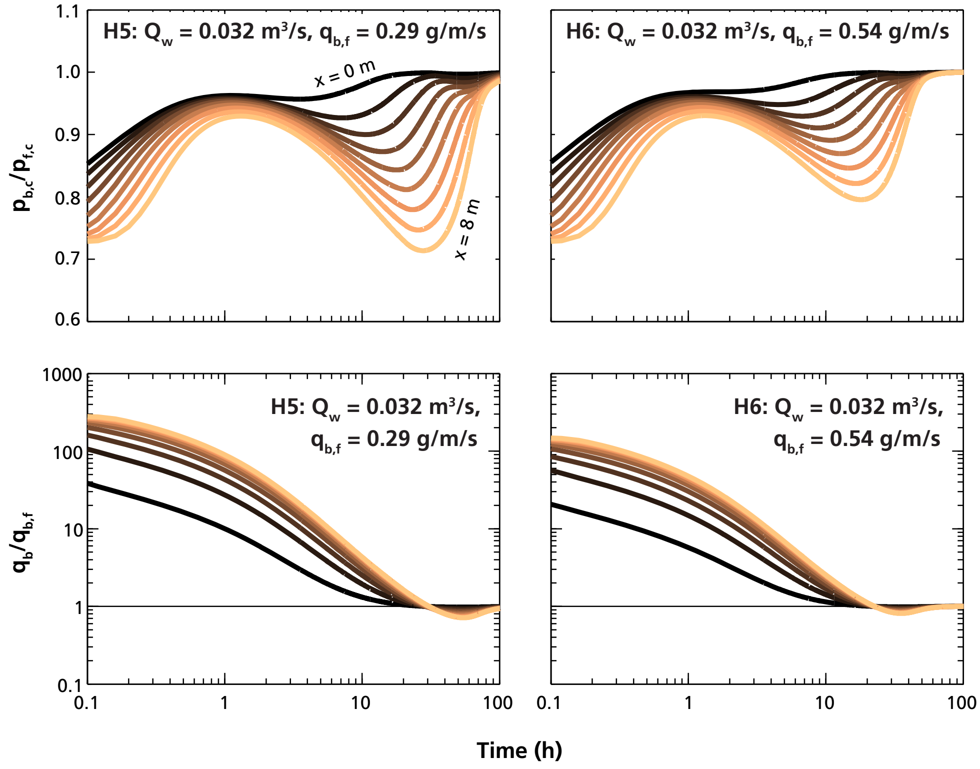

Figure 11. Results of the numerical model for runs H5 and H6. (top) Temporal evolution of the ratio between the gravel fraction of bed load and that fraction of the feed rate. (bottom) Temporal evolution of ratio between the sediment transport rate q_b over the feed rate $q_{b,f}$. Numerical simulations presented at eight cross sections of the flume 1 m apart: the darker the curve, the more upstream the cross section plotted.

texture, the smaller the difference between the sand and coarse ratios (the smaller the amplitude of the bed load fractions), (ii) none of the curves follow an asymptotic trend toward 1 with time, i.e., peaks and troughs are evident in all plots, and (iii) the sand bed load fraction starts below the feed value only for the finest texture (moved 2, Figure 1). Sand and gravel fraction ratios oscillate through time as equilibrium are approached. Figure 13 shows the numerical results of the bed elevation in the channel at specific times for the four textures considered in Figure 12. For comparison, the initial bed elevation has been included in all

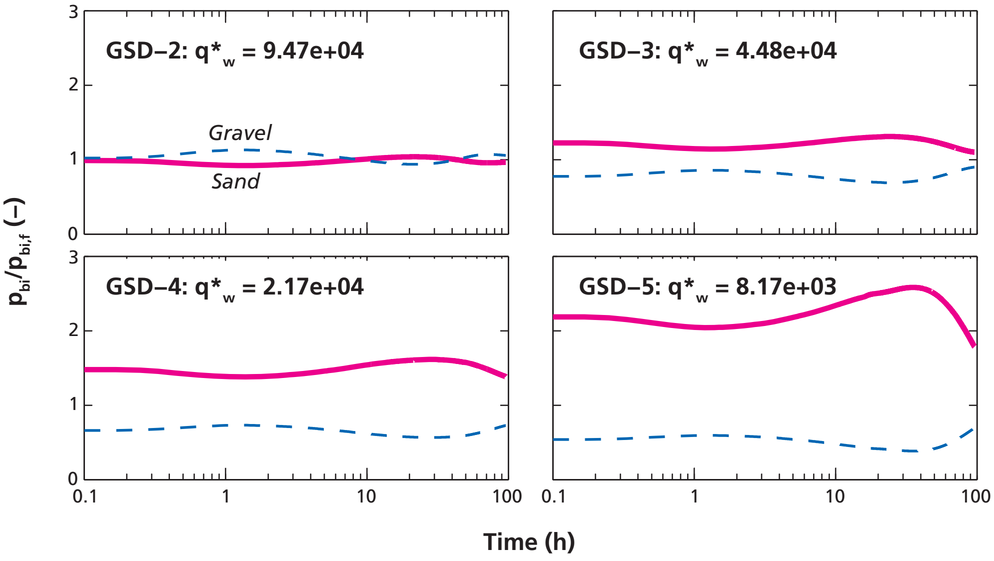

Figure 12. Temporal evolution of the ratio between the sand and gravel bed load fractions at the outlet over the respective feed fractions when the feed rate is $q_{b,f} = 0.55$ g/m/s and the water discharge $Q_w = 0.032$ m^3/s with the four coarsest textures of Figure 9.

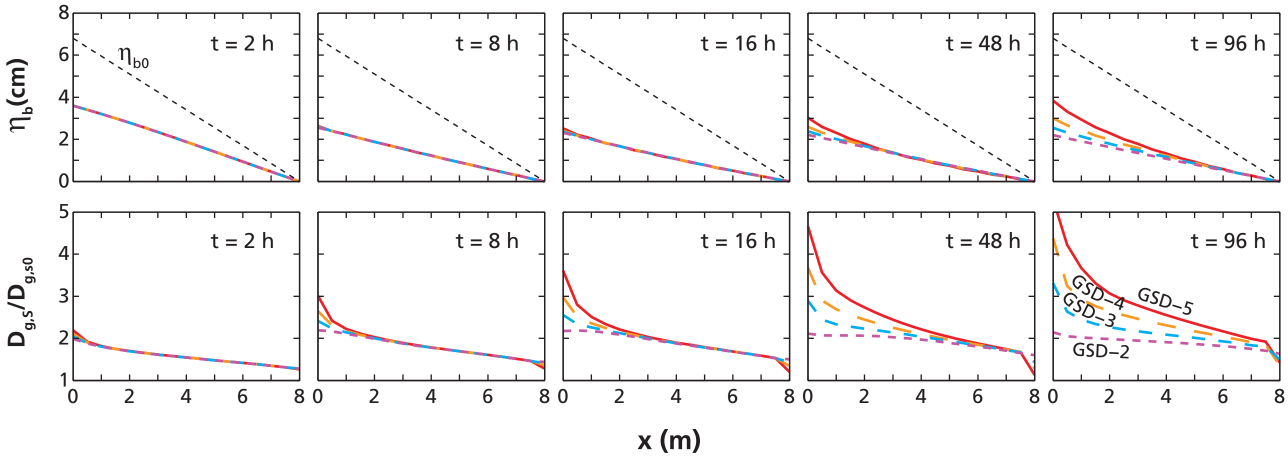

Figure 13. (top) Numerical results of the bed elevation at five specific times ($t = 2$ h, $t = 8$ h, $t = 16$ h, $t = 48$ h, $t = 96$ h). Dashed line in each of the top plots is the initial bed elevation, common for all runs and feed textures. (bottom) Numerical results of the armour ratio (geometric mean diameter on the surface $D_{g,s}$ over its initial value at the same four cross sections $D_{g,s0}$. Results are presented for the four coarsest grain sizes. Statistics of each texture are listed in the inset plot of Figure 9.

top five plots. Figure 13 (bottom) illustrates the numerical results of the surface armor ratio at the same times. The five plots highlight the existing link between the differences in mobility illustrated in Figure 12 and the aggradation in the flume during the final stages of the runs, i.e., the formation of the upstream wedge of sediment: the stronger the difference in mobility among the grain sizes contained in the feed texture, the higher and the earlier the sediment wedge develops. Differences in mobility among the grain sizes are thought to be caused by the presence of sand on the bed surface, mainly driven by the sand content in the feed texture [*Curran and Wilcock*, 2005]. Figure 13 illustrates how this wedge travels along the flume. This bed elevation response can be interpreted as the passage of a slow wave of coarse sediment traveling downstream: the coarser the feed texture, the coarser the front of the sediment wedge. Slow kinematic waves of sediment were also observed by *Reid et al*. [1985] during bed load transport measurements. Recall that the coarsest fractions supplied (Figure 1) in coarse-fed runs are stored in the upper part of the channel, forming a sediment wedge (Figure 8). This sediment wedge causes a change in the availability of coarse material along the flume (provoked by longitudinal sediment sorting) which, as reported by *Iseya and Ikeda* [1987], is thought to be the cause of the bed load oscillations observed. Numerical results in Figure 13 also point out that the surface adjustments to the feed texture are produced faster than those of bed profile: whereas the wave of coarse material is clearly noticed at $t = 8$ h, bed profiles remain insensible to feed texture at this time; it is not until $t = 16$ h when a slight difference in bed profile is observed.

Results of this research can be useful for river researchers and managers. Infiltration of fine material between the gravel interstices affects riverine ecosystems, alters sediment transport, and modifies channel-bed adjustments. As demonstrated herein, the rate and the texture of the sediment supply influences the way by which equilibrium is attained. But more interestingly they also control the adjustment processes of a gravel-bed river in response to the grain size distribution of the feed: (i) by promoting infiltration of fine particles underneath the surface formed by a coarse framework or (ii) by enhancing the mobility of the coarse grain fractions on the bed surface due to the abundance of sand.

Disturbances to gravel-bed streams caused by episodic landslides or debris flows entail large amounts of sediment, the composition of which may be different than that of the bed. As seen, channel response to these disturbances depends on the magnitude and texture of the sediment inputs, as well as the time elapsed between these discrete pulses and on the antecedent channel conditions. Under these conditions, it becomes crucial to know whether the time elapsed between sediment pulses is such that the river can attain equilibrium or, on the contrary, it is not long enough for the river to recover to prepulse conditions. Our experiments were performed under steady flow and sediment supply. Thus, they cannot be used to inform about the critical times between successive episodic inputs of sediment for a channel to reach equilibrium. However, our research contributes reporting the required times to attain equilibrium depending on the texture of the sediment supply in gravel-bed streams with episodic pulses of sediment where (i) the frequency of these pulses is high enough to consider them as a constant supply of sediment and (ii) their magnitude and texture are similar in time. Long-lasting numerical simulations have been carried out under steady flow and sediment feed rate (with a constant duration of 576 h, i.e., six times the duration of the experimental runs). The four coarsest textures of Figure 9 have been used under $Q_w = 0.032$ m^3/s and feed rate $q_{b,f} = 0.55$ g/m/s. Under these conditions, the theoretical bed slope and the surface grain size distribution at equilibrium have been back-calculated using the *Wilcock and Crowe* [2003] equation and following the methodology proposed by *Parker and Wilcock* [1993] imposing that the bed load transport rate and its texture must match those the feed. The degree of equilibrium achievement is defined by the ratio of the surface grain size distribution, feed rate, and its texture at $t = 576$ h over those values at equilibrium at the flume outlet (the last node in attaining equilibrium). Numerical results show that whereas run GSD-2 is nearly at equilibrium at $t = 576$ h ($q_b = 0.99\ q_{b,f}$ and $D_{g,b} = 0.99\ D_{g,f}$), run with GSD-5 is far from such conditions (the sediment transport rate and its geometric mean diameter are 81% lower and 81% finer, respectively, than those of the feed). The same trend is observed with respect to the geometric mean diameter of the bed surface: the ratios between $D_{g,s}$ and those at equilibrium are 0.89 and 0.79 for GSD-2 and GSD-5, respectively. Results of numerical simulations with $Q_w = 0.021$ m^3/s and feed rate $q_{b,f} = 0.15$ g/m/s point out to the same trends: $q_b = 1.06\ q_{b,f}$ and $D_{g,b} = 0.98\ D_{g,f}$ for GSD-2 (i.e., nearly at equilibrium) whereas $q_b = 0.78\ q_{b,f}$ and $D_{g,b} = 0.42\ D_{g,f}$ for GSD-5. It is worth noting that the slightly higher bed load transport rate obtained for run with GSD-2 compared to the feed rate confirms our findings with regards to the oscillations of bed load transport rate around the feed exposed in Figures 9, 11, and 12. From these results, it can be inferred that in rivers with frequent episodic inputs of sediments and given a flow discharge and a feed rate, the coarser the composition of the sediment supply, the longer to achieve equilibrium. Hence, given the results of $D_{g,s}$, q_b, and $D_{g,b}$ at the end of the 576 h long numerical tests compared to those at equilibrium, it can be stated that gravel-bed streams in valleys with frequent landslides or debris flows may not be ever in equilibrium conditions and may always be in a transient stage adjusting to successive discrete events. These long-term simulations point out that, at least for the conditions tested (flow and feed rates, feed textures, and bed slopes), large amounts of time are needed to achieve equilibrium. From the procedural point of view in laboratory studies, long-term measurements should be taken to properly assure that an experiment has reached equilibrium conditions. More research is needed, however, to better understand the role played by the texture of the sediment supply in the temporal adjustments to equilibrium.

5. Conclusions

The influence of the texture of the sediment supply on adjustments in gravel-bed rivers has been experimentally studied. Numerical results confirm the experimental findings. Differences in the sand and gravel fractions in the feed texture result in distinct channel adjustments. Experiments demonstrate that the surface coarsening is controlled by the presence or absence of coarse gravel in the feed texture which can enhance the probability of kinematic sorting of the fine grain sizes by the increase of coarse particles on the surface. Fine sand continuously infiltrates underneath the surface in moved and coarse-supplied runs because of the gravel that is constantly being supplied. This results in increasing surface coarsening during the first 16 h of each run; from this time onward, bed load transport rates match the feed without substantial surface coarsening in moved-supplied runs whereas bed load transport rate and its texture are, respectively, below and much finer than those of the feed in coarse-supplied runs. On the other hand, whereas fine material in low flow sand-supplied runs infiltrates during the first 16 h, it remains on the bed surface once the near-surface pores are saturated. This causes the surface to coarsen in the first phase and to subsequently fine thereafter. It is worth noting that surface coarsening is observed, regardless of the feed texture, when flow strength increases. The experiments also demonstrate that when surface coarsening occurs, no persistent trends in the surface coarsening development are noticed after the first 16 h.

Results of a one-dimensional numerical model demonstrate that longitudinal surface evolution proceeds differently when coarse partially mobile material constitutes a significant proportion of the feed texture (coarse-supplied runs): a wedge of sediment develops in the uppermost part of the channel. This bed aggradation reflects the passage of a slow wave of coarse sediment traveling downstream. This results in a change in the availability of coarse material in the lower sections of the flume which causes bed load oscillations. Results of the numerical tests provide evidence that under weak bed load transport conditions, the higher the differences in mobility among the finest and the coarsest fractions of the feed texture, the higher the amplitudes of the bed load oscillations toward equilibrium. Further, numerical results show that the higher these differences, the more time is needed to achieve equilibrium. These results are significant for gravel-bed stream subjected to episodic sediment inputs, the frequency of which may prevent the river from recovering or achieving equilibrium.

Appendix A

This appendix presents the temporal evolution of the bed load transport rate (Figure A1), the evolution of the D16, D50 and D84 of the bed load transport (Figure A2) and the temporal evolution of the D16, D50 and D84 of the surface texture (Figure A3).

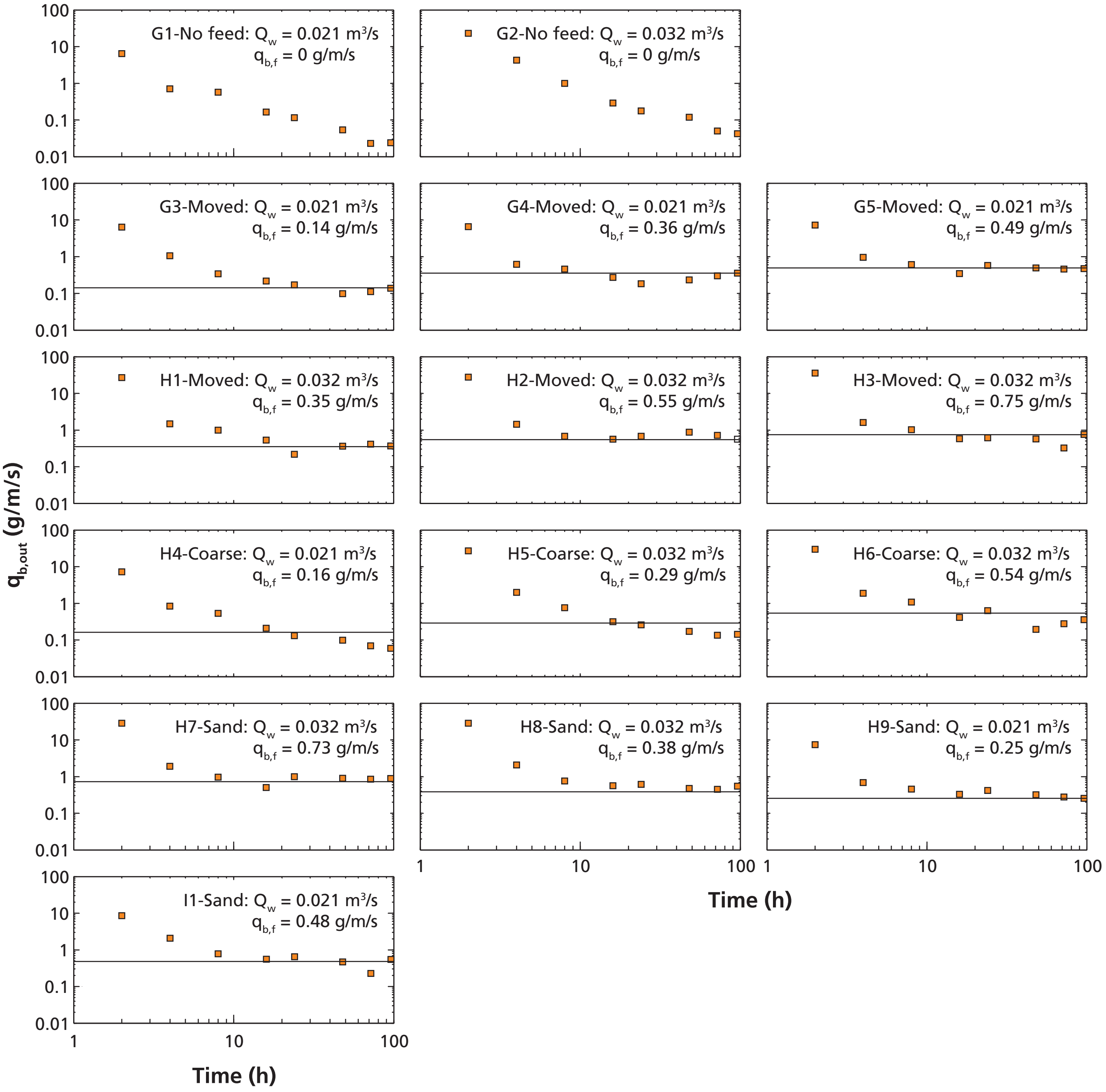

Figure A1. Temporal evolution of the bed load transport rates for all runs.

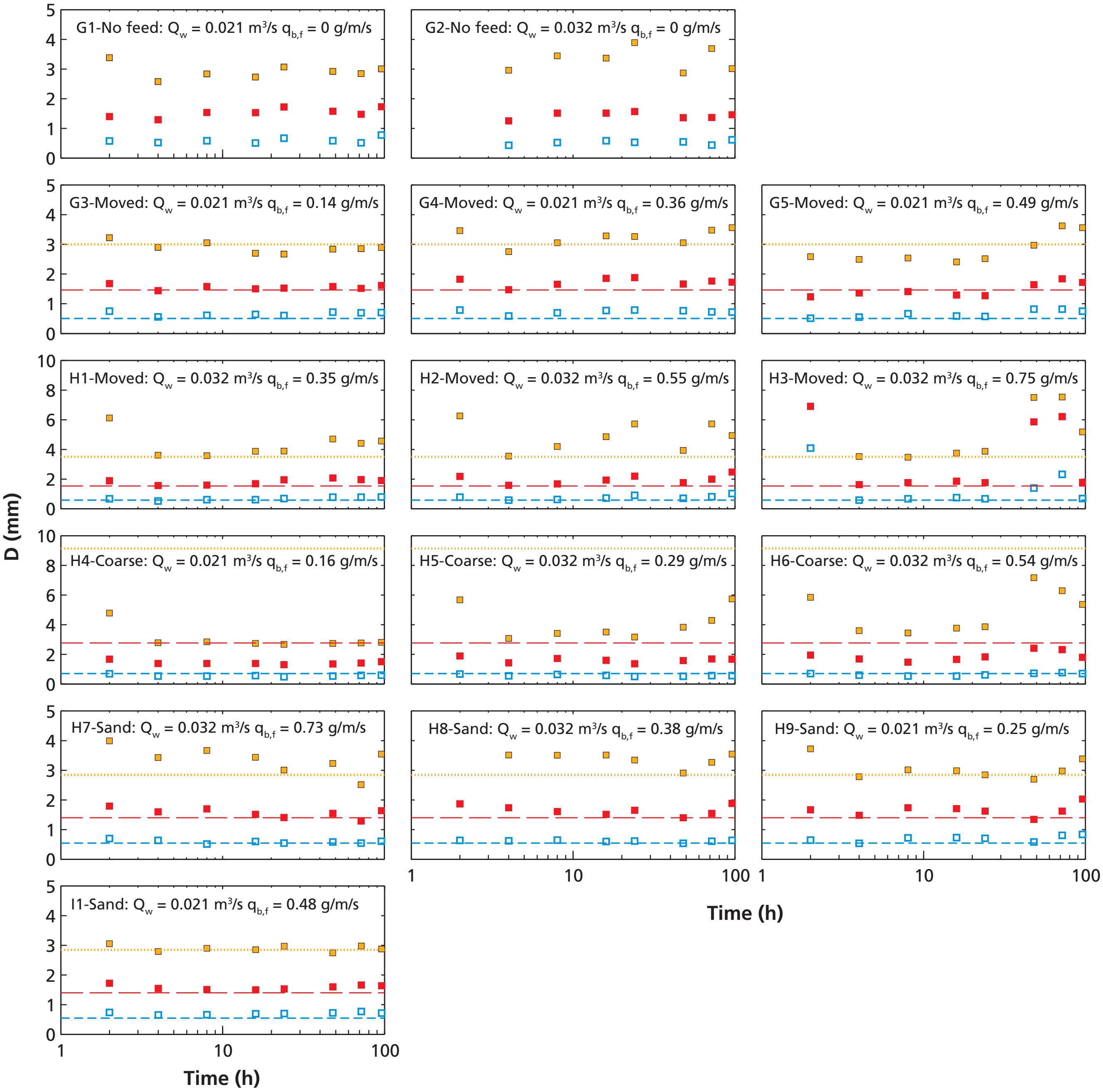

Figure A2. Bed load position statistics for all runs: $D_{16,b}$ (open squares), $D_{50,b}$ (red squares), and $D_{84,b}$ (yellow squares). Dashed lines indicate the values of the respective percentiles of the feed texture.

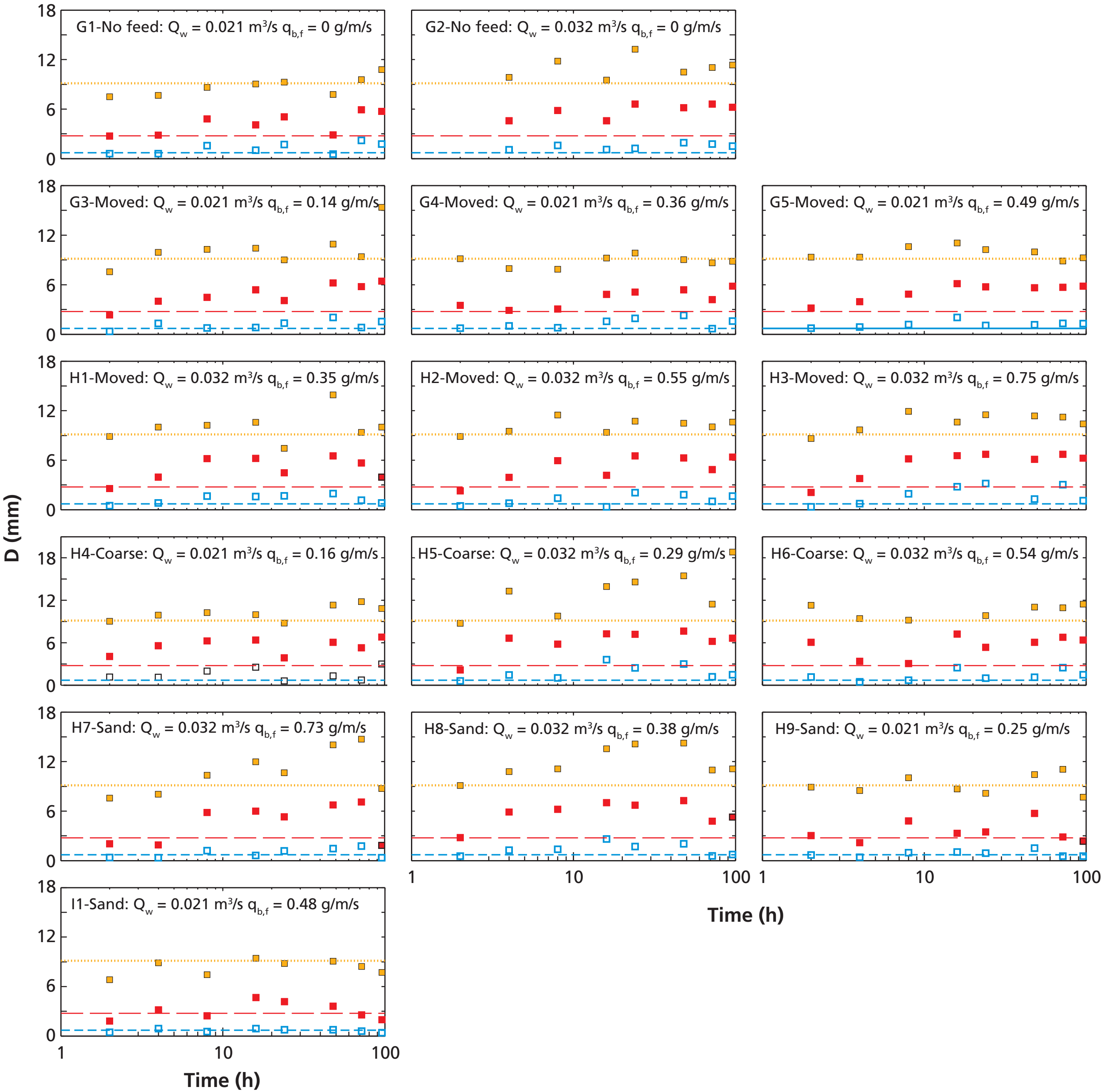

Figure A3. Surface position statistics for all runs: $D_{16,s}$ (open squares), $D_{50,s}$ (red squares), and $D_{84,s}$ (yellow squares). Dashed lines indicate the initial values of the respective percentiles.

Notation

$D_{g,f}$	geometric mean diameter of the feed texture, L.
$D_{g,s}$	geometric mean diameter of the surface texture, L.
$D_{16,b}$	16% percentile of the bed load texture, L.
$D_{16,f}$	16% percentile of the feed texture, L.
$D_{16,s}$	16% percentile of the surface texture, L.
$D_{50,b}$	median diameter of the bed load texture, L.
$D_{50,f}$	median diameter of the feed texture, L.
$D_{50,s}$	median diameter of the bed surface texture, L.

$D_{84,b}$	84% percentile of the bed load texture, L.
$D_{84,f}$	84% percentile of the feed texture, L.
$D_{84,s}$	84% percentile of the bed surface texture, L.
$D_{90,s}$	90% percentile of the surface texture, L.
F_i	i-th fraction of the surface.
$F_{s,f}$	sand content of the feed texture.
g	acceleration of gravity, $L\,T^{-2}$.
p_{bi}	i-th fraction of the bed load transport rate.
p_{bg}	gravel fraction of the bed load transport rate.
p_{bs}	sand fraction of the feed rate.
$p_{b,c}$	coarse fraction of the bed load transport rate when the grain sizes are lumped into two grain classes.
$p_{b,f}$	coarse fraction of the feed rate when the grain sizes are lumped into two grain classes.
$p_{bg,f}$	gravel fraction of the feed rate.
$p_{bs,f}$	sand fraction of the bed load transport rate.
Q_w	water discharge, $L\,T^{-3}$.
q_b	sediment transport rate per unit width, $M\,L^{-1}\,T^{-1}$.
$q_{b,f}$	sediment feed rate per unit width, $M\,L^{-1}\,T^{-1}$.
q_w^*	dimensionless water discharge.
R	submerged specific gravity of the sediment $=(\rho_s-\rho)/\rho$ where ρ and ρ_s are water and sediment density respectively.
t	time, T.
η_b	bed elevation, L.
ρ	water density, $M\,L^{-3}$.
$\sigma_{g,f}$	geometric standard deviation of the feed texture.
τ_b	mean boundary shear stress, $M\,L^{-1}\,T^{-2}$.
τ_g^*	dimensionless shear stress associated with the geometric mean diameter the surface.
τ_{rs84}^*	dimensionless reference shear stress of the 84% percentile of the surface texture.
ψ	grain size on the psi scale; $=\log_2(D)$.

Acknowledgment

The readers can freely access the data from this paper by contacting the first author.

References

Benda, L., and T. Dunne (1997), Stochastic forcing of sediment routing and storage in channel networks, *Water Resour. Res.*, *33*(12), 2849–2863, doi:10.1029/97WR02387.

Buffington, J. M., W. E. Dietrich, and J. W. Kirchner (1992), Friction angle measurements on a naturally formed gravel streambed: Implications for critical boundary shear stress, *Water Resour. Res.*, *28*(2), 411–245, doi:10.1029/91WR02529.

Church, M., and M. A. Hassan (2002), Mobility of bed material in Harris Creek, *Water Resour. Res.*, *38*(11), 1237, doi:10.1029/2001WR000753.

Church, M., M. A. Hassan, and J. F. Wolcott (1998), Stabilizing self-organized structures in gravel-bed stream channels: Field and experimental observations, *Water Resour. Res.*, *34*(11), 3169–3179, doi:10.1029/98WR00484.

Cui, Y., G. Parker, T. E. Lisle, J. Gott, M. E. Hansler-Ball, J. E. Pizzuto, N. E. Allmendinger, and J. M. Reed (2003a), Sediment pulses in mountain rivers: 1. Experiments, *Water Resour. Res.*, *39*(9), 1239, doi:10.1029/2002WR001803.

Cui, Y., G. Parker, J. E. Pizzuto, and T. E. Lisle (2003b), Sediment pulses in mountain rivers: 2. Comparison between experiments and numerical predictions, *Water Resour. Res.*, *39*(9), 1240, doi:10.1029/2002WR001805.

Curran, J. C., and P. R. Wilcock (2005), Effect of sand supply on transport rates in a gravel-bed channel, *J. Hydraul. Eng.*, *131*(11), 961–967, doi:10.1061/(ASCE)0733-9429(2005)131:11(961).

Dietrich, W. E., J. W. Kirchner, H. Ikeda, and F. Iseya (1989), Sediment supply and the development of the coarse surface layer in gravel-bedded rivers, *Nature*, *340*, 215–217, doi:10.1038/340215a0.

Dietrich, W. E., P. A. Nelson, E. Yager, J. G. Venditti, and M. P. Lamb (2005), Sediment patches, sediment supply, and channel morphology, in *River Coastal and Estuarine Morphodynamics RCEM 2005*, edited by P. Gary and M. H. Garcia, pp. 79–90, Taylor and Francis, London, U. K.

Fripp, J., and P. Diplas (1993), Surface sampling in gravel streams, *J. Hydraul. Eng.*, *119*(4), 473–490, doi:10.1061/(ASCE)0733-9429(1993)119:4(473).

Frostick, L. E., P. M. Lucas, and I. Reid (1984), The infiltration of fine matrices into coarse-grained alluvial sediments and its implications for stratigraphical interpretation, *J. Geol. Soc. London*, *141*(6), 955–965, doi:10.1144/gsjgs.141.6.0955.

Gessler, J. (1970), Self-stabilizing tendencies of alluvial channels, *J. Waterw. Harbors Coastal Eng. Div. Am. Soc. Civ. Eng.*, *96*(2), 235–249.

Gilbert, G. K. (1917), Hydraulic-mining débris in the Sierra Nevada, *U.S. Geol. Surv. Prof. Pap. 105*, 154 pp.

Hassan, M. A., and M. Church (2000), Experiments on surface structure and partial sediment transport on a gravel bed, *Water Resour. Res.*, *36*(7), 1885–1895, doi:10.1029/2000WR900055.

Hassan, M. A., R. Egozi, and G. Parker (2006), Experiments on the effect of hydrograph characteristics on vertical grain sorting in gravel bed rivers, *Water Resour. Res.*, *42*, W09408, doi:10.1029/2005WR004707.

Hassan, M. A., B. J. Smith, D. L. Hogan, D. S. Luzi, A. E. Zimmermann, and B. C. Eaton (2008), Sediment storage and transport in coarse bed streams: Scale considerations, in *Gravel-Bed Rivers VI: From Process Understanding to River Restoration*, edited by M. Rinaldi, H. Habersack, and H. Piégay, pp. 473–496, Elsevier, Amsterdam.

Haynes, H., and G. Pender (2007), Stress history effects on gradded bed stability, *J. Hydraul. Eng.*, *133*(4), 343–349, doi:10.1061/(ASCE)0733-9429(2007)133:4(343).

Hoey, T. B. (1992), Temporal variations in bedload transport rates and sediment storage in gravel-bed rivers, *Prog. Phys. Geogr.*, *16*(3), 319–338.

Hoffman, D. F., and E. J. Gabet (2007), Effects of sediment pulses on channel morphology in a gravel bed river, *Geol. Soc. Am. Bull.*, *119*, 116–125.

Iseya, F., and H. Ikeda (1987), Pulsations in bedload transport rates induced by a longitudinal sediment sorting: A flume study using sand and gravel mixtures, *Geogr. Ann., Ser. A*, *69*(1), 15–27.

Kuhnle, R. A., and J. B. Southard (1988), Bed load transport fluctuations in a gravel bed laboratory channel, *Water Resour. Res.*, *24*(2), 247–260, doi:10.1029/WR024i002p00247.

Lisle, T. E. (1989), Sediment transport and resulting deposition in spawning gravels, north coastal California, *Water Resour. Res.*, *25*(6), 1303–1319, doi:10.1029/WR025i006p01303.

Madej, M. A., D. G. Sutherland, T. E. Lisle, and B. Pryor (2009), Channel responses to varying sediment input: A flume experiment modeled after Redwood Creek, California, *Geomorphology*, *103*, 507–519, doi:10.1016/j.geomorph.2008.07.017.

Nelson, P. A., J. G. Venditti, W. E. Dietrich, J. W. Kirchner, H. Ikeda, F. Iseya, and L. S. Sklar (2009), Response of bed surface patchiness to reductions in sediment supply, *J. Geophys. Res.*, *114*, F02005, doi:10.1029/2008JF001144.

Nelson, P. A., W. E. Dietrich, and J. G. Venditti (2010), Bed topography and the development of forced bed surface patches, *J. Geophys. Res.*, *115*, F04024, doi:10.1029/2010JF001747.

Parker, G., and P. Klingeman (1982), On why gravel bed streams are paved, *Water Resour. Res.*, *18*(5), 1409–1423, doi:10.1029/WR018i005p01409.

Parker, G., and A. J. Sutherland (1990), Fluvial armor, *J. Hydraul. Res.*, *28*(5), 529–544.

Parker, G., and P. R. Wilcock (1993), Sediment feed and recirculating flumes: Fundamental difference, *J. Hydraul. Eng.*, *119*(11), 1192–1204.

Parker, G., S. Dhamotharan, and H. Stefan (1982), Model experiments on mobile, paved gravel bed streams, *Water Resour. Res.*, *18*(5), 1395–1408, doi:10.1029/WR018i005p01395.

Pender, G., T. B. Hoey, C. Fuller, and I. K. McEwan (2001), Selective bedload transport during the degradation of a well sorted graded sediment bed, *J. Hydraul. Res.*, *39*(3), 269–277, doi:10.1080/00221680109499830.

Piedra, M., H. Haynes, and T. B. Hoey (2012), The spatial distribution of coarse surface grains and the stability of gravel river beds, *Sedimentology*, *59*, 1014–1029, doi:10.1111/j.1365-3091.2011.01290.x.

Podolak, C. J. P., and P. R. Wilcock (2013), Experimental study of the response of a gravel streambed to increased sediment supply, *Earth Surf. Processes Landforms*, *38*(14), 1748–1764, doi:10.1002/esp.3468.

Pryor, B. S., T. E. Lisle, M. D. Sutherland, and D. Hilton (2011), Transport and storage of bed material in a gravel-bed channel during episode of aggradation and degradation: A field and flume study, *Earth Surf. Processes Landforms*, *36*, 2028–2041, doi:10.1002/esp.2224.

Reid, I., L. E. Frostick, and J. T. Layman (1985), The incidence and nature of bedload transport during flood flows in coarse-grained alluvial channels, *Earth Surf. Processes Landforms*, *10*(1), 33–44, doi:10.1002/esp.3290100107.

Rosato, A., K. J. Strandburg, F. Prinz, and R. H. Swendson (1987), Why the brazil nuts are on top: Size segregation of particulate matter by shaking, *Phys. Rev. Lett.*, *58*(10), 1038–1040, doi:10.1103/PhysRevLett.58.1038.

Sklar, L. S., J. Fadde, J. G. Venditti, P. A. Nelson, M. A. Wydzga, Y. Cui, and W. E. Dietrich (2009), Translation and dispersion of sediment pulses in flume experiments simulating gravel augmentation below dams, *Water Resour. Res.*, *45*, W08439, doi:10.1029/2008WR007346.

Venditti, J. G., W. E. Dietrich, P. A. Nelson, M. A. Wydzga, J. Fadde, and L. Sklar (2010), Mobilization of coarse surface layers in gravel-bedded rivers by finer gravel bed load, *Water Resour. Res.*, *46*, W07506, doi:10.1029/2009WR008329.

Venditti, J. G., P. A. Nelson, J. T. Minear, J. Wooster, and W. E. Dietrich (2012), Alternate bar response to sediment supply termination, *J. Geophys. Res.*, *117*, F02039, doi:10.1029/2011JF002254.

Whiting, P. J., W. E., Dietrich, L. B. Leopold, T. G. Drake, and R. L. Shreve (1988), Bedload sheets in heterogeneous sediment, *Geology*, *16*, 105–108.

Wilcock, P. R. (1998), Two-fraction model of initial sediment motion in gravel-bed rivers, *Science*, *280*(410), doi:10.1126/science.280.5362.410.

Wilcock, P. R. (2001), The flow, the bed, and the transport: Interaction in flume and field, in *Gravel-Bed Rivers V*, edited by M. P. Mosley, pp. 183–220, N. Z. Hydrol. Soc., Wellington, New Zealand.

Wilcock, P. R., and J. C. Crowe (2003), Surface-based transport model for mixed-size sediment, *J. Hydraul. Eng.*, *129*(2), 120–128, doi:10.1061/(ASCE)0733-9429(2003)129:2(120).

Wilcock, P. R., and T. DeTemple (2005), Persistence of armor layers in gravel-bed streams, *Geophys. Res. Lett.*, *32*, L08402, doi:10.1029/2004GL021772.

Wilcock, P. R., and B. W. McArdell (1993), Surface-based fractional transport rates: Mobilization thresholds and partial transport of a sand-gravel sediment, *Water Resour. Res.*, *29*(4), 1297–1312, doi:10.1029/92WR02748.

Wilcock, P. R., S. T. Kenworthy, and J. C. Crowe (2001), Experimental study of the transport of mixed sand and gravel, *Water Resour. Res.*, *37*(2), 3349–3358, doi:10.1029/2001WR000683.

Wooster, J. K., S. R. Dusterhoff, Y. Cui, L. S. Sklar, W. E. Dietrich, and M. Malko (2008), Sediment supply and relative size distribution effects on fine sediment infiltration into immobile gravels, *Water Resour. Res.*, *44*, W03424, doi:10.1029/2006WR005815.